Forschungszentrum Karlsruhe
in der Helmholtz-Gemeinschaft

Wissenschaftliche Berichte
FZKA 7368
SARNET CORIUM P008

SARNET Benchmark on QUENCH-11

Final Report

A. Stefanova, T. Drath, J. Duspiva, W. Erdmann, F. Fichot, G. Guillard, P. Groudev, W. Hering, T. Hollands, Ch. Homann, M. K. Koch, L. Sepold, M. Steinbrück, J. Stuckert, K. Trambauer, A. Vasiliev

Institut für Materialforschung
Institut für Reaktorsicherheit
Programm Nukleare Sicherheitsforschung

März 2008

Forschungszentrum Karlsruhe
in der Helmholtz-Gemeinschaft

Wissenschaftliche Berichte

FZKA 7368

SARNET CORIUM P008

SARNET Benchmark on QUENCH-11
Final Report

A. Stefanova (benchmark coordinator)[1], T. Drath[2], J. Duspiva[3], W. Erdmann[4], F. Fichot[5], G. Guillard[5], P. Groudev[1], W. Hering, T. Hollands[2], Ch. Homann, M. K. Koch[2], L. Sepold, M. Steinbrück, J. Stuckert, K. Trambauer[4], A. Vasiliev[6]

Institut für Materialforschung
Institut für Reaktorsicherheit
Programm Nukleare Sicherheitsforschung

[1]Bulgarian Academy of Sciences, Inst. for Nuclear Research and Nuclear Energy, Sofia
[2]Ruhr-Universität Bochum, Energy Systems and Energy Economics
[3]Dept. of Reactor Technology, Nuclear Research Institute Rez plc, Czech Republic
[4]Gesellschaft für Anlagen- und Reaktorsicherheit (GRS), Garching
[5]Institut de Radioprotection et de Sûreté Nucléaire, France (IRSN), Cadarache
[6]Russian Academy of Sciences, Nuclear Safety Institute (IBRAE), Moscow

Forschungszentrum Karlsruhe GmbH, Karlsruhe

2008

Forschungszentrum Karlsruhe GmbH
Postfach 3640, 76021 Karlsruhe

Mitglied der Hermann von Helmholtz-Gemeinschaft
Deutscher Forschungszentren (HGF)

ISSN 0947-8620

urn:nbn:de:0005-073682

Zusammenfassung

SARNET-Benchmark des Versuchs QUENCH-11 - Abschlussbericht

In den QUENCH-Versuchen wird der Wasserstoffquellterm bei der Einspeisung von Notkühlwasser in einen trockenen, überhitzten Reaktorkern eines Leichtwasserreaktors untersucht. Ferner wird in den Versuchen das Verhalten von überhitzten Brennelementen unter verschiedenen Flutbedingungen untersucht, eine Datenbasis zur Modellentwicklung und eine Weiterentwicklung von Rechenprogrammen zu Schweren Störfällen (engl. SFD – Severe Fuel Damage) erstellt.

Der Ausdampf-Versuch QUENCH-11 wurde am 8. Dezember 2005 durchgeführt. Es war das zweite Experiment im Rahmen des EU-geförderten LACOMERA-Programms. Es sollte einen Kühlmittelpumpenausfall während eines Kühlmittelverluststörfalls (hier ein sog. Small Break LOCA) oder einer plötzlichen Stromabschaltung (eng. „station blackout“) mit einer späten Druckentlastung des Primärsystems simulieren. Verbunden mit dem Unfallszenario ist das Ausdampfen eines teilgefüllten Reaktorkerns bzw. des Versuchsbündels. Das Ziel war die Untersuchung des Bündelverhaltens während des Ausdampfens und des nachfolgenden Abschreckens mit reduzierter Wassereinspeiserate. Es war das erste Experiment, in dem der gesamte Unfallablauf von der Ausdampfphase bis zur verzögerten Flutung des Bündels bei einer geringen Wasser-Einspeiserate untersucht werden sollte. Das Ausmaß der Wechselwirkungen von Thermalhydraulik und Materialien war in dem Experiment ausgeprägter als in früheren QUENCH-Versuchen. Das Experiment wurde von INRNE Sofia (Bulgarische Akademie der Wissenschaften) vorgeschlagen und zusammen mit dem Forschungszentrum Karlsruhe definiert.

Nach dem Experiment wurde entschieden, die QUENCH-11-Daten für ein Rechenprogramm-Benchmark, bei dem die Rechenergebnisse mit den experimentellen Daten verglichen werden, im Rahmen des Europäischen Exzellenz-Netzwerks SARNET anzubieten, um die Zuverlässigkeit der Rechnungen für die verschiedenen Phasen von Unfall bzw. Experiment zu überprüfen. Die eingesetzten SFD-Rechenprogramme waren ASTEC, ATHLET-CD, ICARE-CATHARE, MELCOR, RATEG/SVECHA, RELAP/SCDAPSIM, and SCDAP/RELAP5. Die Koordination für den Vergleich übernahm INRNE.

Als Grundlage für den Vergleich dienten die zeitlichen Verläufe von Temperaturen, Wasserstofferzeugung und anderer wichtiger Daten. Außerdem wurden Axialprofile, in erster Linie die der Temperatur zum Zeitpunkt des Flutbeginns und des Endstadiums, d. h. bei der Testzeit von 7000 s, verglichen. Für die meisten Rechenergebnisse kann ein gemeinsamer Trendverlauf angegeben werden. Größere Unterschiede zeigen die Ergebnisse für die Wasserstofferzeugung und die zugehörige Oxidschichtdicke.

Der Grad der Übereinstimmung zwischen Rechnung und Experiment wird von den Schwachstellen der Rechnung und des Experiments gleichermaßen mitbestimmt. SFD-Rechenprogramme sind zur Analyse von typischen Kernreaktorunfällen entwickelt worden. Einzelne Besonderheiten der experimentellen Anordnung integraler Experimente (wie auch QUENCH-11) sind bedingt durch das Vorhandensein von Dampfführungsrohr (Shroud) und Elektrodenmaterial für die elektrische Stabheizung nicht reaktortypisch und können daher

nicht in der gewünschten Einzelheit im Rechenprogramm nachgebildet werden. Hinzu kommen Effekte durch den Anwender. Da jedoch die Bandbreite der wesentlichen Rechenergebnisse einschließlich der Wasserstofferzeugung nicht extrem groß ist, kann das Ergebnis des SFD-Rechenprogramm-Benchmarks insgesamt als positiv bewertet werden.

Ein Vergleich mit anderen Experimenten zeigt einen weiteren Bedarf an Verbesserungen besonders im Hinblick auf die Oxidation stark zerstörter Bündelstrukturen während des Flutens.

Zusätzlich erwies sich das Rechenprogramm-Benchmark für einige Programmanwender als wertvoll, um sich mit den physikalischen Problematiken und der Anwendung von großen SFD-Rechenprogrammen vertraut zu machen. Es dient dem Erfahrungsaustausch mit jüngeren Wissenschaftlern und Ingenieuren und der Aufrechterhaltung des Standards der nuklearen Sicherheit.

Abstract

The QUENCH out-of-pile experiments at Forschungszentrum Karlsruhe (Karlsruhe Research Center) are set up to investigate the hydrogen source term that results from the water or steam injection into an uncovered core of a Light-Water Reactor, to examine the behavior of overheated fuel elements under different flooding conditions, and to create a database for model development and improvement of Severe Fuel Damage (SFD) code packages.

The boil-off experiment QUENCH-11 was performed on December 8, 2005 as the second of two experiments in the frame of the EC-supported LACOMERA program. It was to simulate ceasing pumps in case of a small break LOCA or a station blackout with a late depressurization of the primary system, starting with boil-down of a test bundle that was partially filled with water. It is the first test to investigate the whole sequence of an anticipated reactor accident from the boil-off phase to delayed reflood of the bundle with a low water injection rate. The test is characterized by an interaction of thermal-hydraulics and material interactions that is even stronger than in previous QUENCH tests. It was proposed by INRNE Sofia (Bulgarian Academy of Sciences) and defined together with Forschungszentrum Karlsruhe.

After the test, QUENCH-11 was chosen as a SARNET code benchmark exercise. Its task is a comparison between experimental data and analytical results to assess the reliability of the code prediction for different phases of an accident and the experiment. The SFD codes used were ASTEC, ATHLET-CD, ICARE-CATHARE, MELCOR, RATEG/SVECHA, RELAP/-SCDAPSIM, and SCDAP/RELAP5. The INRNE took responsibility as benchmark coordinator to compare the code results with the experimental data.

As a basis of the present work, histories of temperatures, hydrogen production and other important variables were used. Besides, axial profiles at quench initiation and the final time of 7000 s, above all of temperatures, are presented. For most variables a mainstream of computational results can be defined. Larger discrepancies are seen in the hydrogen production and the related oxide scale thickness.

Analysis shows that the agreement between calculated and experimental data is determined by both, limitations of severe accident codes and of the experiment. Severe accident codes are intended and developed to analyze typical accident situations in nuclear reactors. Special features of the experimental set-up of integral tests like QUENCH-11 as the presence of a shroud and electrode materials for the electric heating are irrelevant for reactors and cannot be simulated in the desirable detail. User effects add to the problems. However, a limited bandwidth of some calculated mainstream results, including hydrogen production, is a good outcome of the code benchmark. Taking in view other experiments, a further demand for an improvement concerning the oxidation of severe damaged structures during a reflood scenario is seen.

Additionally, the benchmark proved to be valuable for a number of participants to become acquainted with the physical problems and with the application of large severe accident codes. For the transfer of knowledge and experience to younger scientists and engineers, this is an important issue to maintain the standard of nuclear safety.

Contents

List of Tables

List of Figures

List of Abbreviations

CORIUM	SARNET working package
DC	Direct Current
EC	European Commission
FZK	Forschungszentrum Karlsruhe
GRS	Gesellschaft für Anlagen- und Reaktorsicherheit, Germany
IBRAE	Nuclear Safety Institute, Russian Academy of Science
IMF	Institut für Materialforschung, Forschungszentrum, Karlsruhe
INR	Institute for Nuclear Research, Romania
INRNE	Institute for Nuclear Research and Nuclear Energy, Sofia, Bulgaria
IRSN	Institut de Radioprotection et de Sûreté Nucléaire, France
ISP	International Standard Problem
ISS	Innovative Systems Software, USA
LACOMERA	Large Scale Experiments on Core Degradation, Melt Retention and Coolability
LP	Lower Plenum
LWR	Light Water Reactor
NRI	Nuclear Research Institute, Czech Republic
NUKLEAR	Programm Nukleare Sicherheitsforschung, Forschungszentrum Karlsruhe
OECD	Organization for Economic Co-operation and Development
PWR	Pressurized Water Reactor
RUB-LEE	Ruhr-Universität Bochum, Department for Energy Systems and Energy Economics, Germany
SA	Severe Accident
SARNET	Severe Accident Research Network of Excellence
SFD	Severe Fuel Damage
SNL	Sandia National Laboratories, USA
CNSNS	Comisión Nacional de Seguridad Nuclear y Salvaguardias, Mexico
TC	Thermocouple
UZ	University of Zagreb, Croatia

Introduction

The QUENCH experiments at the Karlsruhe Research Center are set up to investigate the hydrogen source term that results from the water or steam injection into an uncovered core of a Light-Water Reactor (LWR), to examine the behavior of overheated fuel elements under different flooding conditions, and to create a database for model development and improvement of Severe Fuel Damage code packages.

The test QUENCH-11 was to simulate ceasing pumps in case of a small break LOCA or a station blackout with a late depressurization of the primary system. It started with boil-down of a bundle that was partially filled with water. So far, no integral experiment has been performed with a controlled evaporation of a free water surface in the test section, neither for reactor-operating nor for non-power conditions. The small reflood rate addresses the situation, when only few injection systems are available. The test is characterized by an interaction of thermal-hydraulics and material interactions that is even stronger than in previous QUENCH tests.

This test was proposed by INRNE (Institute for Nuclear Research and Nuclear Energy), Bulgarian Academy of Sciences, Sofia, and defined together with the Karlsruhe Research Center and conducted at the Karlsruhe Research Center on 8th December 2005 as the second of two experiments in the frame of the EC-supported LACOMERA program [1]. It is based on extended pretest calculations prior to several QUENCH-11 pretests [3] and the main test [14]. After the test, it was chosen as a SARNET benchmark exercise. Its task is defined as a comparison between QUENCH-11 experimental data and analytical results received from the different computer codes to assess the reliability of the code prediction for different phases of an accident and the experiment.

The comparison of the code results with experimental data was performed by INRNE in the frame of the SARNET program [10]. The experimental data supplied to the participants to perform their calculations were limited to the data sets for initial and boundary conditions and a number of results, but not all of them (half-blind problem). Nevertheless, some preliminary results of the QUENCH-11 test were presented before the definition of the QUENCH-11 experiment as SARNET benchmark [6],[7] which were made available to all participants.

This report describes experimental and computational results, compares those results and assesses the qualities of both results.

1 Objectives and Time Schedule

The main benchmark objectives are:

- Investigation of the bundle behavior during boil-off, core heat-up and reflood.

- Check on consistency and accuracy of SA code modeling and comparison of corresponding results as temperature, water evaporation, oxidation, hydrogen release during all test phases with emphasis on the quench phase.

- Bundle end state prediction.

The time schedule is presented in Table 2.1.

Table 2.1: Initial and final time schedule.

Initial time	Events	Final time
October 25-27, 2005	11th International QUENCH Workshop	
December 8, 2005	QUENCH-11 test conduct at FZK	
June, 2006	Definition of the objectives and released data	
July 14, 2006	Participation deadline for delivery draft Final specification benchmark report	July 30, 2006
July-October, 2006	Participant's calculations period	January, 2007
October 24-26, 2006	12th QUENCH Workshop: Presentation of results	October 24-28, 2007
October 30, 2006	Deadline for submission of calculations to coordinator	January 30, 2007
	3rd Annual ERMSAR Review Meeting, GRS Garching, Germany	January 29-Febr. 2, 2007
	Final ERMSAR Review Meeting in Karlsruhe	June 12-14, 2007
May, 2007	Final QUENCH-11 Benchmark meeting in Karlsruhe	June 15, 2007
August, 2007	First draft of benchmark final report	September 20, 2007
October, 2007	Benchmark final report	January, 2008

2 Description of the QUENCH Facility

The overall description of the QUENCH facility is provided in several FZK reports [5]. This report includes some additional information on the QUENCH-11 experiment. The overview of flow paths including water and gas inlets and outlets, and boundary conditions are presented in Figure 3.1.

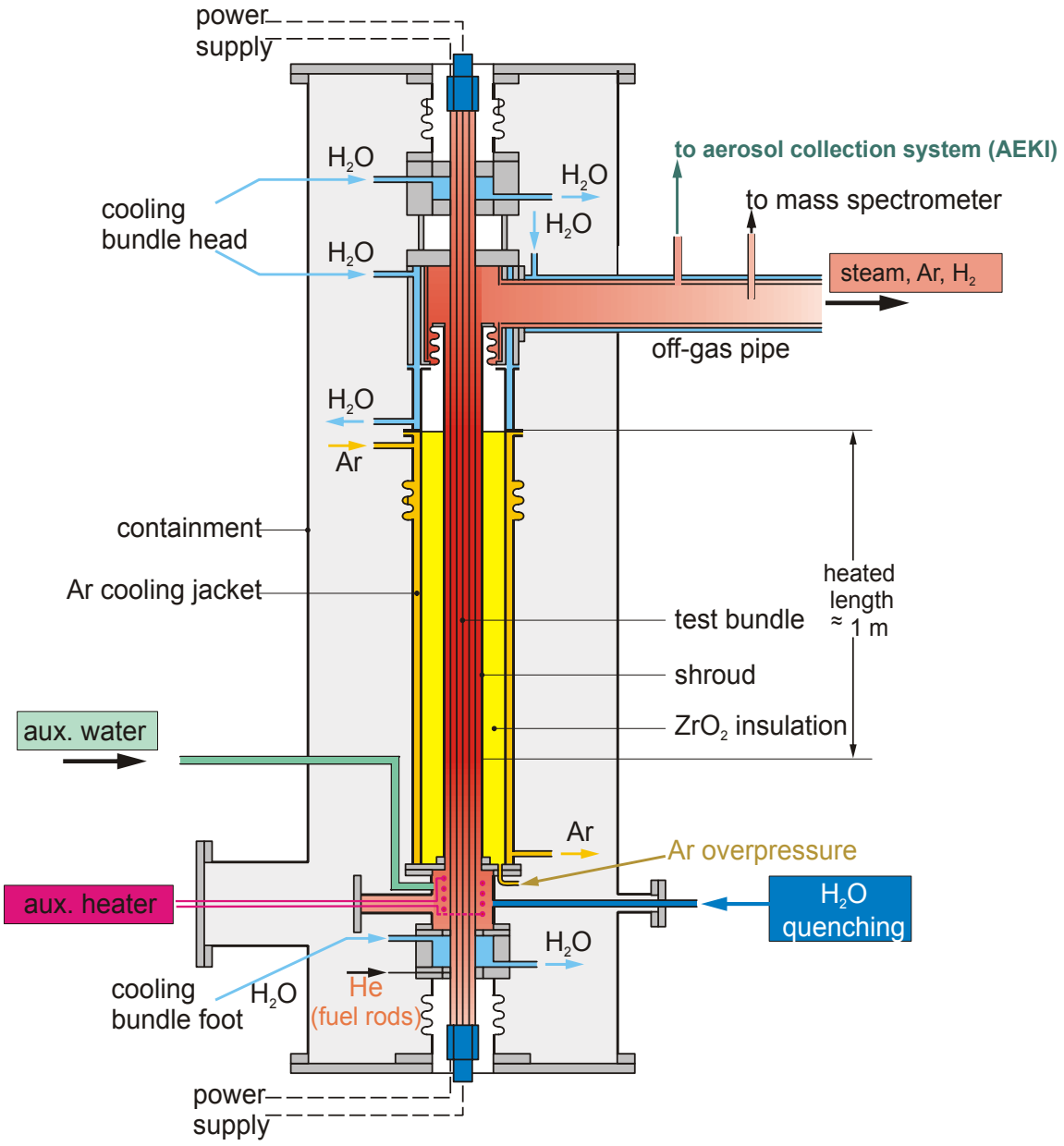

Figure 3.1: Overview of flow paths of the QUENCH test section with fuel rod simulator bundle, shroud, cooling jacket (argon and water cooling), fill gas for the fuel rods as well as water cooling at the axial ends of the electrodes.

2.1 Inlet Section

The geometry of the test section inlet is presented in Figure 3.2. In the QUENCH-11 test section the inlet pipe was closed at the flange and an auxiliary water feeding line was added as indicated in this figure. The flow distributor in the lower bundle plenum is modified and contains an auxiliary heater with a resistance of 16.6 Ω which can be controlled between 0.1 and 3.5 kW so that the evaporation rate and the heatup rate in the bundle can be controlled independently. The approximate locations of the thermocouples of this region are indicated.

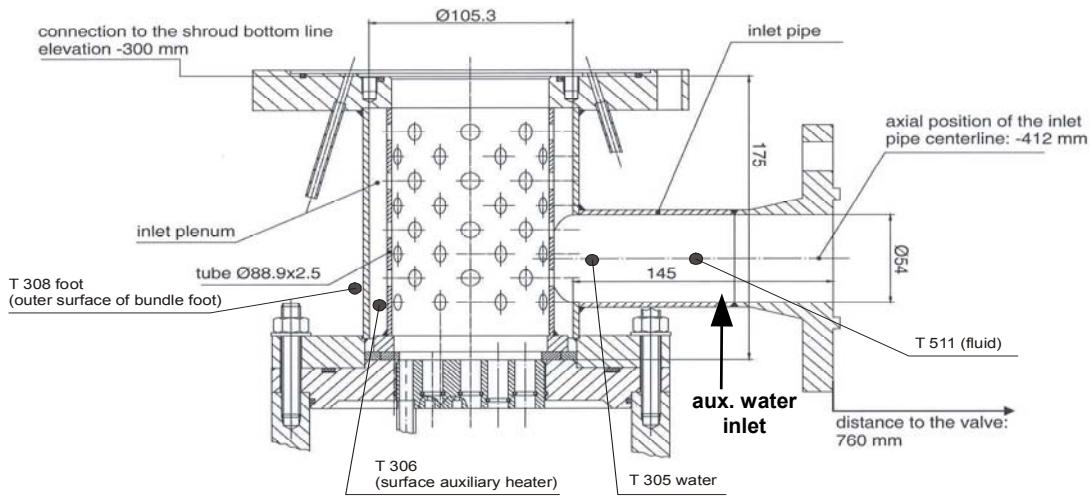

Figure 3.2: Test section inlet modified for QUENCH-11: auxiliary heater, additional temperature measurement devices, and auxiliary water inlet.

2.2 Bundle Test Section

The test bundle is made up of 21 fuel rod simulators with a total length of approximately 2.5 m. Bundle geometry and clad material correspond to Western commercial LWRs. Details are given in Table 3.1. Except the central one all rods are heated over a length of 1024 mm. Heating is electric by 6 mm diameter tungsten heaters installed in the rod center. Electrodes of molybdenum/copper are connected to the tungsten heaters at one end and to the cable leading to the DC electrical power supply at the other end. The heating power is distributed between two groups of heated rods. The distribution of the electric power within the two groups is as follows: about 40 % of the power is released into the inner rod circuit consisting of eight fuel rod simulators (in parallel connection) and 60 % in the outer rod circuit (12 fuel rod simulators in parallel connection). The measured electric resistance of a single heater (W+Mo+Cu sections) is 3 mΩ at room temperature. This value increases significantly with temperature. The additional resistance of the external electric circuit between the axial end of the single heater and the connection to the generator (sliding contacts, cables, and bolts) is 1.46 mΩ + 0.22 mΩ = 1.68 mΩ. This value can be taken as constant because the external electric circuit remains at room temperature throughout the experiment.

The fuel rod simulators are held in position by five grid spacers, four are made of Zircaloy and the one at the bottom of Inconel. Different to all previous tests the location of the two lowest spacers was changed. The exact locations are provided in Table 3.1. Annular ZrO_2 pellets surround the tungsten heaters. The rod cladding of the heated fuel rod simulator is identical to that used in LWRs with respect to material and dimensions except the length. All test rods, including the central one, are filled with He with approx. 0.22 MPa pressure. The rods are connected to a feeding system that allows observation of a first cladding failure by mass spectroscopy. Two fuel rod simulators were made with duplex claddings of the "DX-D4" type. There are four Zircaloy corner rods installed in the bundle. Two of them, i.e. rods "A" and "C" are made of a solid Zry rod at the top and a Zry tube at the bottom and are used for thermocouple instrumentation whereas the other two rods, i.e. Rods "B" and "D" (solid Zry rods of 6 mm diameter) can be withdrawn from the bundle to check the amount of ZrO_2 oxidation at pre-defined times. The bundle cross section with the different rod groups is presented in Figure 3.3. The test bundle is surrounded by a shroud of Zircaloy with a 37 mm thick ZrO_2 fiber insulation [2] from the bottom to the upper end of the heated zone and a double-walled cooling jacket of stainless steel over the entire length (see also Figure 3.1). The annulus between shroud and cooling jacket was filled with stagnant argon of 0.22 MPa. It was connected to a flow- and pressure-controlled argon feeding system in order to keep the pressure constant at the target of 0.22 MPa (pressure release above this value) and to prevent an access of steam to the annulus after shroud failure (argon feeding below the target value). The 6.7 mm annulus of the cooling jacket is cooled by an argon flow up to the upper end of the heated zone. The cooling jacket is surrounded by a safety containment with a thickness of 5.6 mm. Inner and outer diameter of the containment amount to 801.8 and 813 mm, respectively.

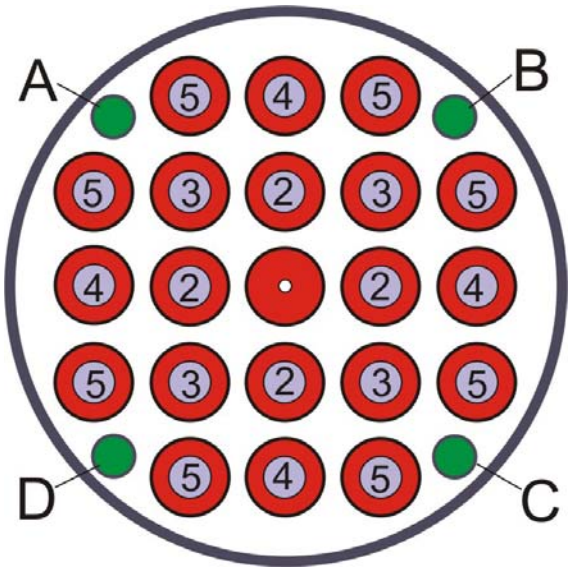

Figure 3.3: Bundle cross section with designation of the rod groups.

Table 3.1: Design characteristics of the QUENCH-11 test bundle.

Bundle type		PWR
Bundle size		21 rods
Number of heated rods		20
Number of unheated rods		1
Pitch		14.3 mm
Coolant channel area		30.1 cm^2
Hydraulic diameter		11.6 mm
Rod outside diameter		10.75 mm
Cladding material		Zircaloy-4 *)
Cladding thickness		0.725 mm
Rod length	heated rod (levels) unheated rod (levels)	2480 mm (-690 mm to 1790 mm) 2842 mm (-827 mm to 2015 mm, incl. extension piece)
Heater material		Tungsten (W)
Heater length		1024 mm
Heater diameter		6 mm
Annular pellet	material heated rod unheated rod	ZrO_2;Y_2O_3-stabilized ∅ 9.15/6.15 mm; L=11 mm ∅ 9.15/2.5 mm; L=11 mm
Pellet stack	heated rod unheated rod	0 mm to ~ 1020 mm 0 mm to 1553 mm
Corner rod (4)	material instrumented not instrumented (solid)	Zircaloy-4 tube ∅ 6x0.9 (bottom: -1140 mm) rod ∅ 6 mm (top: +1300 mm) rod ∅ 6 mm (-1350 to +1155 mm)
Grid spacer	material length location of lower edge	Zircaloy-4, Inconel 718 Zry 42 mm, Inc 38 mm -100 mm Inconel 150 mm Zircaloy-4 550 mm Zircaloy-4 1050 mm Zircaloy-4 1410 mm Zircaloy-4
Shroud	material wall thickness outside diameter length (extension)	Zircaloy-4 2.38 mm 84.76 mm 1600 mm (-300 mm to 1300 mm)
Shroud insulation	material insulation thickness elevation	ZrO_2 fiber ~ 37 mm -300 mm to ~1000 mm
Molybdenum-copper electrodes	length of upper electrodes length of lower electrodes diameter of electrodes: - prior to coating - after coating with ZrO_2	766 mm (576 Mo, 190 mm Cu) 690 mm (300 Mo, 390 mm Cu) 8.6 mm 9.0 mm
Cooling jacket	Material: inner/outer tube inner tube outer tube	Inconel 600 (2.4816)/SS (1.4571) ∅ 158.3 / 168.3 mm ∅ 181.7 / 193.7 mm

*) Rods # 14 and 20 use a duplex cladding of the type “DX-D4” with a Zry-4 base material (thickness 575 µm) and an external liner (thickness 150 µm).

2.3 Test Section Outlet

The test section outlet is presented in detail in Figure 3.4.

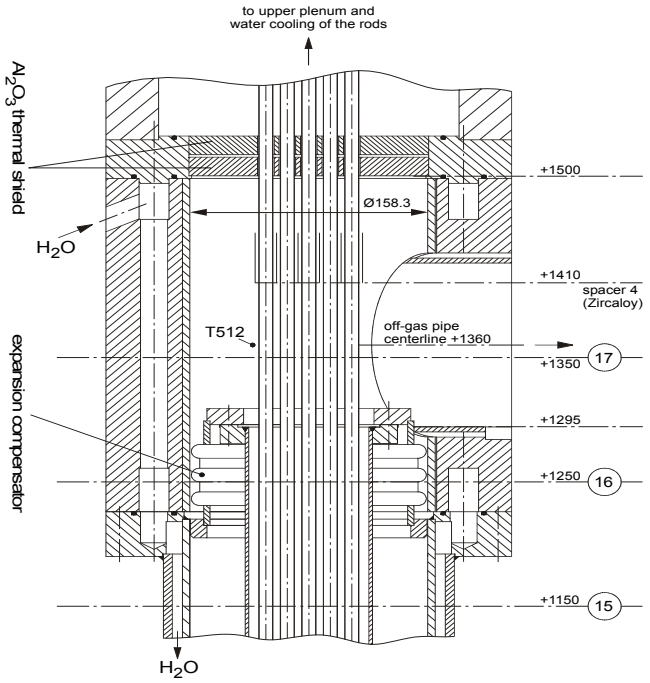

Figure 3.4: QUENCH test section outlet.

A temperature control unit was added to the water cooling circuit of the bundle head to keep the temperature there at 348 K. The flow rate of the cooling water was 250 g/s.

2.4 Off-gas Pipe

The off-gas pipe consists of a water-cooled inner pipe for the fluid leaving the bundle. The water cooling is a countercurrent flow within the cooling jacket of the off-gas pipe with a flow rate of 370 g/s. The inlet temperature is controlled at 393 K to guarantee that the steam/gas temperature is high enough so that condensation of the off-gas can be avoided. There are two annuli within the off-gas pipe: Cooling water flows in parallel to the off-gas through the outer annulus whereas the inner one is connected to the inner tube so that it is filled with almost stagnant off-gas.

3 QUENCH-11 Main Instrumentation

Hydrogen is analyzed by two different measurement systems: (1) a state-of-the-art mass spectrometer Balzers “GAM300” located at the off-gas pipe ~2.70 m downstream the test section, (2) a commercial-type hydrogen detection system ”Caldos 7 G” by Hartmann&Braun located at the end of the off-gas line, i.e. downstream the condenser. Due to the different locations in the facility the mass spectrometer “GAM 300” responds almost immediately to changes in the gas composition whereas the Caldos device has a delay time of about 20-30 s. With the mass spectrometer all off-gas species including steam can be analyzed whereas the Caldos system works only for binary Ar/H_2 mixtures. The argon carrier gas was injected at the bundle head throughout the entire QUENCH-11 experiment.

For **temperature** measurements the test bundle, shroud, and cooling jackets are equipped with thermocouples at 17 elevations and different orientations.

The thermocouples attached to the outer surface of the rod cladding at elevations between -250 and 1350 mm are designated “TCR” for the central rod and “TFS” for all other rods. “TCRC” is the designation for the thermocouples installed at the 550 and 950 mm levels at the center of the central rod. The shroud thermocouples (designation “TSH”) are mounted at the outer surface between -250 mm and 1250 mm. The thermocouples that are installed inside the Zircaloy instrumentation rods at the two corner positions of the bundle (positions A and C) are designated “TIT”. The thermocouples of the cooling jacket are installed inside the wall of the inner cooling tube (from -250 mm to 1150 mm, designation “TCI”) and at the outer surface of the outer cooling tube (from -250 mm to 950 mm, designation “TCO”).

In the lower bundle region, i.e. up to 550 mm elevation, standard-type thermocouples with an outside diameter of 1.0 mm are used for measurements of the rod cladding, rod centerline and shroud temperatures. The thermocouples in the hot zone and above are high-temperature thermocouples with an outside diameter of 2.1 mm. The thermocouples of the cooling jacket (TCI and TCO) are 1 mm standard-type thermocouples for all levels.

In general, it was avoided to route the TC cables of those TCs through the hot zone. The cables of shroud thermocouples TSH were routed outside the shroud insulation.

Electrical bundle power is derived from measured electric current and voltage. The voltage measurement is done outside the bundle and includes the voltage drop at the sliding contacts at both ends of the rods, at the cables which lead from the sliding contacts to the power supply, and at nuts and bolts that fix the cables at the power supply unit.

The **collapsed water level** is measured by a differential pressure gauge (L 501) connected to the test section at the -409 and +1309 mm bundle elevations.

4 Estimated Accuracies of the Measurements in the QUENCH-11 Experiment

The fuel rod bundle and the shroud are equipped with high-temperature thermocouples at various elevations and positions. The details of mounting and internal structure are provided in the benchmark specification report [4] and in [9].

The general accuracy of thermocouples is better than 2.5 % of the measured temperature. High-temperature thermocouples can be used above 500 K (according to comparative measurements during the QUENCH-13 experiment using NiCr-Ni thermocouples as a reference). As the initial test rod and shroud temperatures were around 400 K in QUENCH-11, i.e. below the 500 K value, maximum differences of 15 % between the different high-temperature thermocouples were recorded. In addition, the individual mounting as well as the fluid environment have to be taken into account. At high temperatures in a gaseous atmosphere the temperatures measured by surface-mounted high-temperature TCs show lower values of up to 50 K compared to the corresponding cladding temperature. In two-phase flow environment the fin effect may become dominant for these TCs (droplets

deposition and evaporation). Internal TCs do not suffer from such effect, but they show a delay due to thermal inertia of surroundings.

The mass spectrometer is calibrated for steady state conditions with certified argon-gas mixtures for the non-condensable gases and with a well-defined argon-steam mixture for steam. The minimum detectable value for H_2O and H_2 is given to 20 ppm, that for other non-condensable gases approx. 1 ppm. The mass spectrometer accuracy is generally better than 5 %, particularly after having installed heating bands at the sampling line to avoid condensation of the steam. It may be worse (30 %) during the highly transient quench phase with high steam and low argon (reference gas) concentrations. The accuracy of the MS during the quench phase with low reflood rates is estimated to be better than 20 %. The time delay of the MS measurement is short; test measurements with hydrogen injection into the bundle resulted in values less than 5 s. According to the manufacturer, the accuracy of the electrical bundle heating is 1 % and of the auxiliary heater 0.5 %.

Accuracy of the water level measurement, L 501, is below 0.1 % of the water level according to the manufacturer, but uncertainty due to oscillations in the two-phase flow regime is by far larger. Before the quench phase, an accuracy of 10 mm is estimated as a rough guide value.

5 The QUENCH-11 Experiment

5.1 Test Conduct

The QUENCH-11 test phases can be summarized as follows.

	Water filling of the bundle to 982 mm elevation. Bundle heat-up to ~383 K.
Phase I	**Boil-off** of the water-filled bundle to -190 mm elevation accompanied by bundle heat-up (~0.3 K/s to ~1480 K).
Phase II	Continued **boil-off** with enhanced bundle heat-up (~0.7 K/s at 1480 to 1830 K and >3 K/s from ~1830 K) with (almost) constant water level.
Phase III	**Quenching** of the bundle by a water flow of 18 (17+1) g/s.

In Phase I (steady boil-off) a top-down uncovery of the test bundle took place until the minimum water level of -190 mm was reached.

In Phase II the steady evaporation continued, and the water level as well as the steam flow was kept fairly stable, i.e. between -190 and -175 mm bundle elevation, by injecting ~1 g/s of 363 K hot water at 2575 s until test termination.

The injection ~1 g/s of water was continued, even during the quench phase (Phase III). The temperatures increased by raising the electric bundle power. An onset of significant cladding oxidation was first detected with help of the hydrogen measurement at 4900 s, the maximum bundle temperatures being approx. 1433 K.

Quenching the bundle was conducted by injecting 17 g/s (plus 1 g/s) of water at 293 K at the bottom of the test section. Bundle temperatures in the hot zone were then ~2000 K. At elevations below 800 mm the progressive filling of the bundle led to a progressive bottom-up quenching, with no significant temperature increase after the initiation of reflood. Locations above 800 mm exhibited an initial and significant temperature excursion causing temperatures to exceed 2400 K. The excursion corresponded to an increase of hydrogen generation and is attributed to the heat produced by an intensive oxidation. The continued water injection was limited by a breach in the shroud, apparently at the 800 mm level. Locations above 850 mm were slowly cooled down after terminating the electrical heating. Temperatures close to saturation were reached after a quenching time of around 3000 s.

Table 6.1: Sequence of the main events of the QUENCH-11 test.

Time, [s]	Events
0	Start data acquisition Bundle at 383 K, Ar flow 3.04 g/s (385 K). Auxiliary power at 0.48 kW.
224	Switch-on of bundle power (~ 6.7 kW). Auxiliary power at 0.36 kW.
1035	Initiation of auxiliary heater power transient.
2578	Start auxiliary water feed (flow rate 1.1 g/s).
5487	Withdrawal of corner rod B.
5500	Quench initiation (increase of F 104 to approx. 17 g/s during next 40 s).
5520	Quench water at test section inlet.
5563	Shroud failure; first test rod failure by helium detection.
5573	Reduction bundle power from 6.8 to 3.9 kW.
5575	Bundle power at decay heat level.
5645	Maximum temperature.
5702	Auxiliary power shut off.
5713	Bundle power shut off.
5795	Water level reached maximum elevation of 868 mm.
6004	Quench pump shut off.
6324	Auxiliary water injection switched off.
8928	End of data acquisition.

After the experiment the QUENCH-11 bundle and its shroud appear severely damaged, i.e. in the region above ~750 mm the shroud and bundle were partially molten, and the shroud was shaped to a large “bubble”, similar to the QUENCH-07 and QUENCH-09 test bundles. A look into the test bundle at ~800 mm elevation showed melt rivulets solidified in the flow channels. From above ~1000 mm the shroud fell off during dismantling. Furthermore, the shroud in the bubble-shaped region is oxidized severely and has reacted with the ZrO_2 fiber insulation (see also Figure 6.1 and Ref. [9]).

5.2 Posttest Status of the Test Bundle by Evaluation of Cross Sections

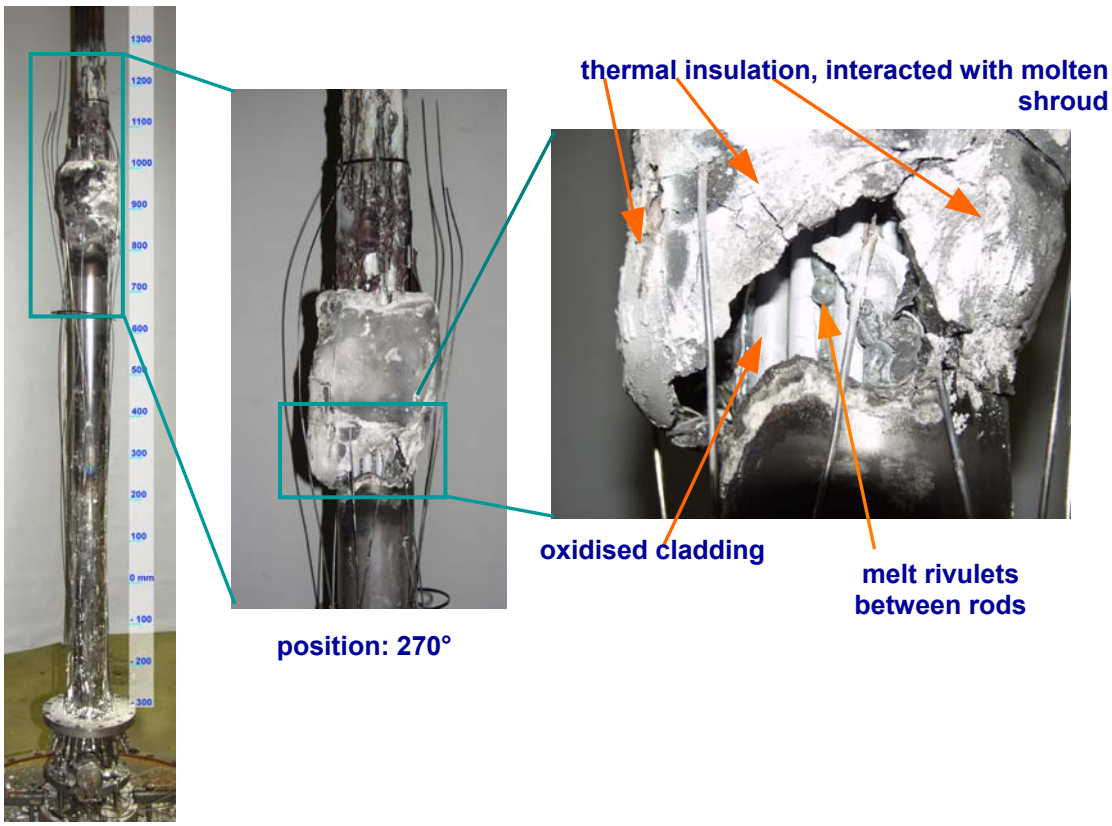

Figure 6.1: Posttest appearance of the QUENCH-11 test bundle at ~750 mm elevation.

The posttest appearance of the bundle at 750 mm elevation is presented in Figure 6.1. Up to about 800 mm the bundle is intact, and the rod claddings show protective external scales of axially increasing thickness. Internal cladding oxidation in contact to pellets is obvious for the 810 mm level, at which gap filling versus void formation due to internal melt relocation took place. Considerable amounts of melt of rod and shroud origin are kept here and above; only small fractions of relocated melt are found down to 750 mm. In its lower range, the partial flow channel blockage has been formed by non-coherent melt candling and re-solidification in consecutive events: Melt rivulet flow proceeded with poor cladding wetting, and pillow formation was favored. Embedded cladding scale got mostly dissolved during the continued growth of scale at the steam exposed surfaces of the metallic melt itself, so that “necks” between rod and melt are formed, surrounded by common scale. Rivulets relocated later are seen to have dissolved covered scale of earlier melt. At other positions voids, which became isolated from steam access, can be distinguished from open flow channels. In the center of the partial blockage and around the elevation 850 mm, an additional melt type was analyzed to contain, besides Zr and Sn from cladding origin, Mo and W from the degradation of electrodes and heater rods, which is obvious at higher elevations. (Both refractory metals are known to form multi-component melts in case of oxidative attack and far below their own melting points.) Here, ceramic residues of converted cladding and the pellets remain without excessive fragmentation.

In the transient and reflood phase of the experiment, the accelerating temperature increase together with the moderate evaporation rate has given rise to a continuing upward movement of the escalation front into the upper electrode zone. This indicates that sufficient steam was

available for oxidation during the entire test. The involvement of facility-specific molten products, the presence of a thick-walled shroud, and the restriction related to the simulation of fuel by zirconium oxide pellets have to be taken into account, but the gained results are qualitatively prototypical: In anticipated LWR accidents of this type, elongated partial blockages of the observed character would be formed, containing considerable fractions of dissolved and thus relocated fuel. In respective refill scenarios, temporal damage progression to higher core elevations would take place.

5.3 Bundle Oxide Thickness Layer

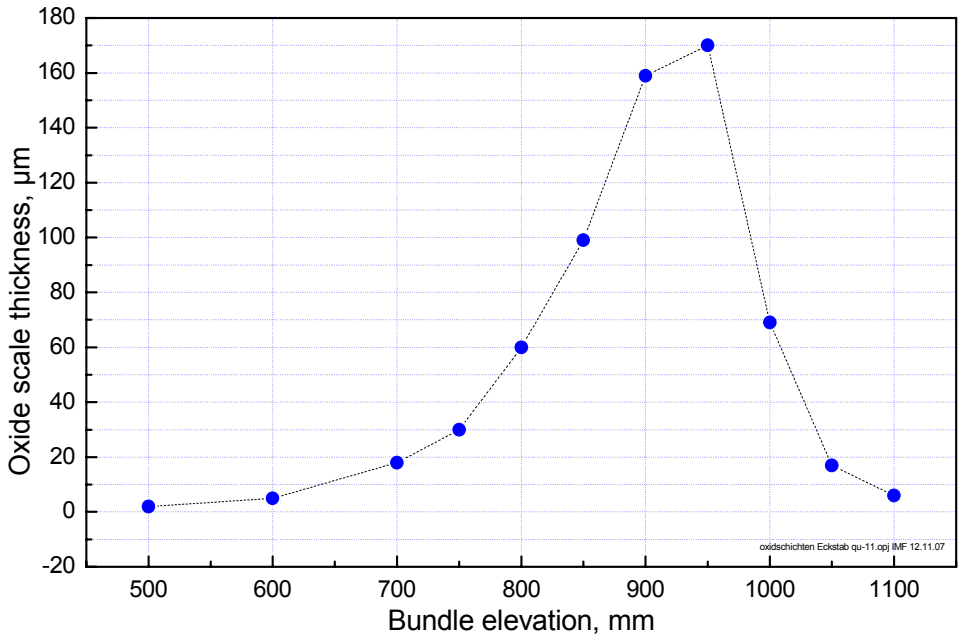

Figure 6.2: Bundle oxide thickness measured at corner rod B prior to the quench phase of the main test QUENCH-11. (After the pretest the corner rod was re-inserted into the test bundle.)

The scale thickness profile gained after the pre-test, for the corner rod B, Figure 6.2 presents the results of the scale thickness measurement, plotted against the axial elevation of the rod in the bundle. The scale thickness profile gained after the pre-test, and that determined for the rod condition after removal near the end of the transient in the main test, give a common peak position at 950 mm elevation.

The determined axial scale thickness profile, as given in Figure 6.3, combines the separate results for simulator rods, corner rods, and shroud inner side with the standard deviation range of the simulator rods. Accordingly, the extent of oxidation is rising steeply from unimportant values for the lower levels to complete cladding oxidation, which is reached for all rods at 900 mm and is maintained in the upper electrode zone.

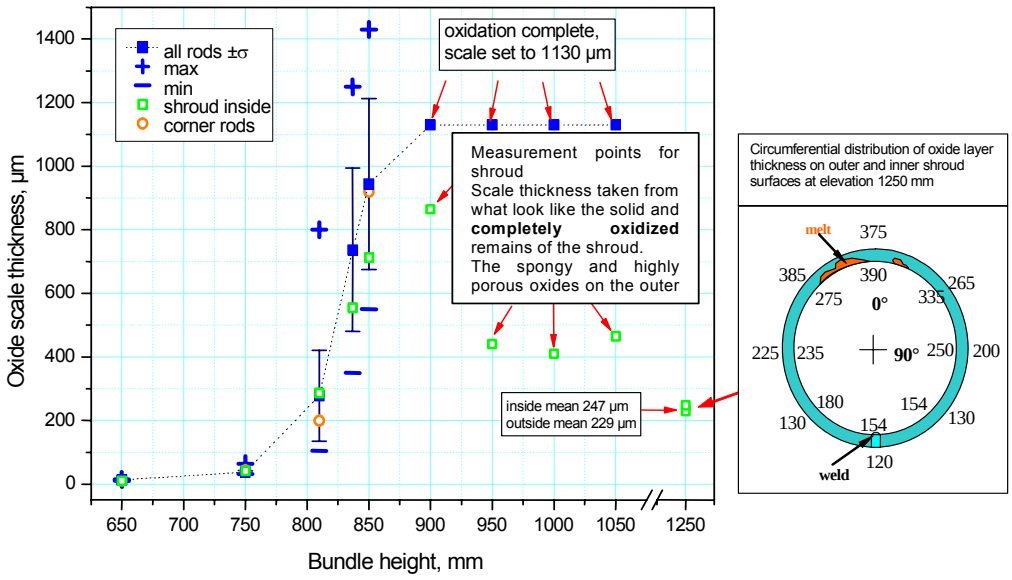

Figure 6.3: QUENCH-11; Posttest axial oxide layer distribution of test rods, corner rods, and shroud.

5.4 Global Assessment of Material Distribution in Selected Cross Sections

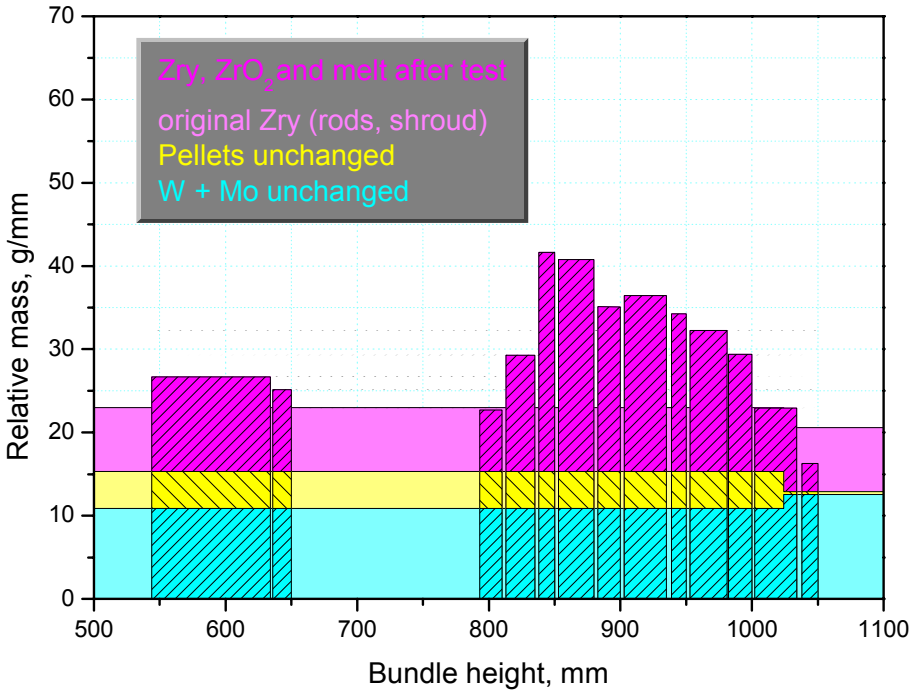

Figure 6.4: Posttest axial mass distribution of bundle material based on epoxy data and sample weights compared to the pretest status.

To determine the area occupied by structural parts (rods, shroud, pellets, melt) in cross-sections along the bundle elevation, the data of the mass of epoxy that has been filled into the bundle have been used. These data were gained by measuring the epoxy consumption for every 10 mm filling level during embedding (see Ref. [9], Table 15). With the known density of the epoxy (1.1 g/cm^3) the volume of it, and therefore the cross-sectional area occupied by it, was calculated in steps of 10 mm. Finally, a very rough axial profile of masses

is obtained by looking at the masses of all cut segments (those intended for polishing and the slabs between them). Figure 6.4 reveals the results of this analysis, which is described in more detail in [9].

A second method for determination of material distribution is direct measurements of areas by means of analysis of the images of selected cross sections (Figures 6.5 - 6.6). The results are presented in Table 6.2. This work has been performed on the polished surfaces at 750, 810, 850, 900, 950, 1000 and 1050 mm. It was also tried to determine the areas of cladding, pellets and heaters because for elevations at 900 mm and above there actually have been changes in pellets and heaters. So wherever possible, up to seven different fractions have been discriminated: Metallic melt of Zircaloy origin between rods, oxidic melt of Zircaloy origin between rods, metallic melt of electrode origin between rods, oxidized cladding, metallic cladding, pellets, and heaters/electrodes. With respect to the shroud, only data of 810 and 850 mm were collected, for higher elevations the influence of the fiber insulation is indeterminate.

Table 6.2: Material distribution based on measurements of areas by means of image analysis.

	1 **Zry cladding** **mm^2**	2 **ZrO_2 cladding (oxide scale)** **mm^2**	3 **Zry melt between rods** **mm^2**	4 **ZrO_2 melt between rods** **mm^2**	3+4 **"debris"** **mm^2**	1+3 **"Zry"** **mm^2**	2+4 **"ZrO_2"** **mm^2**
Below 650 mm	480	0	0	0	0	480	0
650 mm QUE-11-1	475	9	0	0	0	475	9
750 mm QUE-11-2	462	27	36	0	36	498	27
810 mm QUE-11-6	368	158	146	172	318	514	330
850 mm QUE-11-3	32	473	172	564	736	204	1037
900 mm QUE-11-7	0	590	0	303	303	0	893
950 mm QUE-11-4	0	655	0	391	391	0	1046
1000 mm QUE-11-8	0	291	0	330	330	0	621
1050 mm QUE-11-5	0	See column 4	0	744, includes ZrO_2 cladding	(744)	0	744

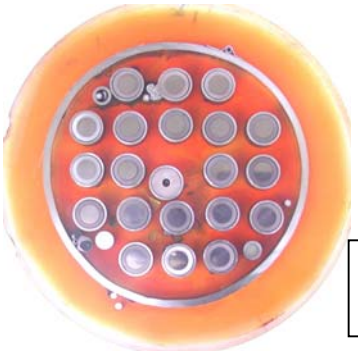

QUE-11-2
750 mm

QUE-11-6
810 mm

QUE-11-3
top
850 mm

Figure 6.5: Color macro photos of cross sections at 750-850 mm for quantification of material distribution by image analysis.

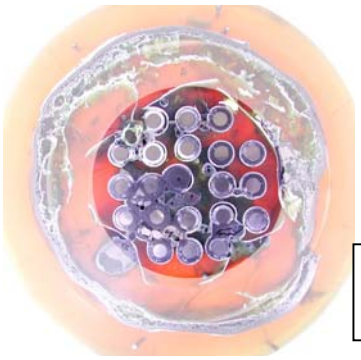

QUE-11-7
900 mm

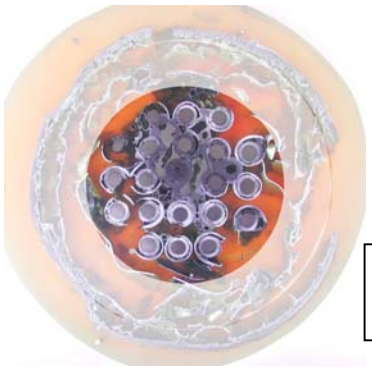

QUE-11-4
950 mm

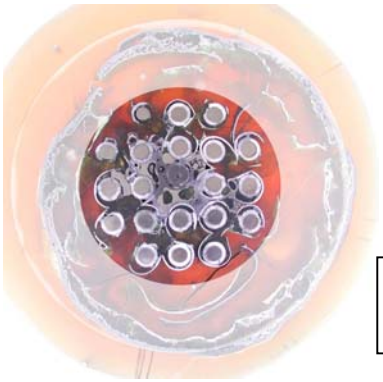

QUE-11-8
1000 mm

QUE-11-5
1050 mm

Figure 6.6: Color macro photos of cross sections at 900-1050 mm for quantification of material distribution by image analysis.

Estimation of the Posttest Flow Channel Area in the Selected Cross Sections

Additionally, an attempt was made to find out something about the remaining fluid channels by analysis of transmitted light through thin bundle cuts. The results are presented in Table 6.3 and described in detail in [9]. Two different data on the flow area, i.e. “data 1” and “data 2”, are provided for the option to include (data 2) or exclude the shroud (data 1) in the code calculations.

Table 6.3: Flow channel area determined from the selected cross sections.

	Fluid flow area; data 1*) mm^2	**Fluid flow area; data 2 mm^2**
Below 650 mm	3036	3036
650 mm QUE-11-1	3036	3036
750 mm QUE-11-2	3000	3000
810 mm QUE-11-6	2240	2240
850 mm QUE-11-3	420	2520
900 mm QUE-11-7	1450	4410
950 mm QUE-11-4	1320	4940
1000 mm QUE-11-8	1580	5580
1050 mm QUE-11-5	1980	--

*) Data 1 are evaluated by assuming that the shroud kept its pretest inner diameter;
Data 2 are evaluated by using the actual posttest dimensions of the shroud.

5.5 Estimation of Hydrogen Production by Oxidation of the Various Bundle Components

Based on all information available on oxidized bundle components, the contributions to the total hydrogen production by oxidation of the various components was estimated according the procedure described in [11]. The sum of hydrogen produced by the oxidation of the various components (143 g; see Table 6.4) is in excellent agreement with the value measured online by mass spectrometer (141 g). **92 g** (64 %) of the hydrogen released was produced by the oxidation of prototypical bundle components, usually considered in SFD code systems, i.e. cladding tubes, corner rods, spacer grids, and inner shroud surface. 51 g of hydrogen resulted from the oxidation of the shroud outer surface and melt, heaters, electrodes and high-temperature thermocouples. This has to be taken into account for comparison of experimental and calculated results.

Table 6.4: **Contributions to the total hydrogen release estimated with help of the posttest bundle status.**

Component	Location	Assumption	H_2, g
Cladding	0-900 mm	interpolation and integration of oxide scale measurements	14
	900-1300 mm	complete oxidation	55
	>1300 mm	rough estimation, no data	5
Corner rods	B (withdrawn)	interpolation and integration of oxide scale measurements	0.1
	A, C, D 0-900 mm	interpolation and integration of oxide scale measurements	1
	A, C 900-1300 mm	complete oxidation of instrumentation tubes	3
	D 900-1150 mm	complete oxidation of rod	1
Shroud	0-1050 mm *inner surface*	interpolation and integration of oxide scale measurements	8
	500-1300 mm *outer surface*	interpolation and integration of oxide scale measurements	8
	1050-1250 mm	80 % oxidation of molten and relocated shroud, excluding the remaining oxide (see line above)	24
Grid spacers	550, 1050, 1410 mm	1x completely oxidized plus small contribution of lower and upper one	5
W heaters	900-1024 mm	from metallography: 2 % consumption and oxidation over a length of 10 cm	1
Mo electrodes	1024-1200 mm	from metallography: 18% molten of which 50 % oxidised over a length of 20 cm	13
HT-TCs	0-900 mm	interpolation and integration of oxide scale measurements at cladding	1
	900-1300, Zry	complete oxidation	2
	900-1300, Ta	complete oxidation	1
Σ			**143**

6 Participants and Codes

6.1 Participants

Requirements for the delivery of the calculated results by the benchmark participants were defined in [4]. Ten participants from seven countries delivered a large variety of data sets as listed in Table 7.1. Typing and other obvious errors were corrected by the coordinator. Some participants did not match the specified time vectors, so that it was not possible to define the plot data as requested. This caused additional efforts and increased the data volume.

Table 7.1: Final list of participants and their organizations.

No	Token	Analysts	Organization	E-mail	Nation
I) Group received all measured data					
1	FZK1	W. Hering	FZK	hering@irs.fzk.de	GER
2	FZK2	Ch. Homann	FZK	homann@irs.fzk.de	GER
3	INRNE	P. Groudev	INRNE-BAS	pavlinpg@inrne.bas.bg	BG
II) Group received limited data information					
4	GRS	W. Erdmann, K. Trambauer	Gesellschaft für Anlagen- und Reaktorsicherheit (GRS)	walter.erdmann@grs.de klaus.trambauer@grs.de	GER
5	IBRAE	A. Vasiliev	IBRAE	vasil@ibrae.ac.ru	RU
6	NRI	J. Duspiva	Nuclear Research Institute	dsp@ujv.cz	CZ
7	RUB-LEE	M. K. Koch	Ruhr-University Bochum	koch@LEE.RUB.de	GER
		T. Hollands		hollands@LEE.RUB.de	
		T. Drath		drath@LEE.RUB.de	
8	IRSN	G. Guillard	Institut de Radioprotection et de Sûreté Nucléaire, Cadarache	gaetan.guillard@irsn.fr	FR
		F. Fichot		bandini@bologna.enea.it	
9	UZ	S. Šadek	University of Zagreb	sinisa.sadek@fer.hr	Croatia
10	INR	G.Negut, A. Catana	Institute for Nuclear Research	joenegut@yahoo.com calex_2002@yahoo.com	RO

6.2 Codes

In the QUENCH-11 benchmark, calculations were performed with the computer codes ASTEC, ATHLET-CD [8], ICARE-CATHARE, MELCOR, RATEG/SVECHA RELAP/SCDAPSIM, and SCDAP/RELAP5.

The codes can be subdivided into two groups:

- Integral code systems (I) and
- Detailed codes (D).

The comparison of the main physical parameters presented by the participants is shown in the Table 7.2.

Table 7.2: Code features.

Code	Code Type	Token	Analysts	Thermal-hydraulic	Clad failure temp. crit.	Oxidation correlation Low/high
SCDAP/ RELAP5	D	FZK1	Ch. Homann	2p, 1*D	2500 K	CP/UH
ASTEC	I	FZK2	W. Hering	2p, 1D	2300 K	L/PC
MELCOR 1.8.5	I	INRNE	P. Groudev	2p, 1D	2500 K	UH
ATHLET-CD 2.1A	D	GRS	W. Erdmann	2p, 1D	2030 K	L/PC
RATEG/ SVECHA	D	IBRAE	A. Vasiliev	2p, 1D	2140 K	CP&LS/PC&LA
MELCOR 1.8.6	I	NRI	J. Duspiva	2p, 1D	2800 K	UH
ATHLET-CD 2.1A	D	RUB-LEE	T. Hollands, T. Drath, M. Koch	2p, 1D	2300 K/ low oxid. 2400 K/ high oxid.	L/PC
ICARE/CATHARE	D	IRSN	G.Guillard, F. Fichot	2p, 1D	2300 K	CP/PC
RELAP/ SCDAPSIM	D	UZ	S. Sadek	2p, 1D	2500 K	CP/UH
RELAP/ SCDAPSIM	D	INR	G.Negut, A. Catana	2p, 1D	2500 K	CP/UH

Thermal hydraulics: p: phase; D: dimension; 1*D: 1D+cross flow dimension

Oxidation correlations: UH: Urbanic-Heidrick; L: Leistikov; PC: Prater/Courtright; LS: Leistikov-Schanz; LA: Leistikov-Aly, CP: Cathcart-Pawel

6.3 General Code Features

The thermal-hydraulic capabilities of different computer codes are briefly described below:

Integral computer codes:

- In ASTEC, the thermal-hydraulic front end is the module CESAR. In the related model, two phases, water and gas (steam + H_2), are considered. The numerical approach is a 5-equation model: 2 mass equations, 2 energy equations and 1 equation for steam velocity with a drift flux correlation for water velocity. The state variables are: total pressure, void fraction, steam enthalpy, water enthalpy, partial pressure of H_2, and steam velocity. However, CESAR should only be applied below temperatures of 700 K. For this reason, it was not used in this benchmark. Instead, the thermal-hydraulic model of DIVA was applied. It is focused on the needs of in-core simulations and has a 1-D approach for liquid water and a 2-D approach for steam.

- The MELCOR computer code uses representation of two-phase thermal-hydraulics with two independent momentum equations. The major distinction from more detailed codes is the use of a “flow regime map” for coupling the phases by exchange of momentum. MELCOR’s “map” is simple, and is only intended to give good results for the limits of counter-current flow and low-velocity entrainment.

Detailed computer codes:

- The detailed computer code ATHLET-CD uses a 5-equation representation of two-phase thermal-hydraulics for this calculation. The single momentum equation is extended by a drift flux correlation coupling both phases.

- The ICARE/CATHARE is based on the French thermal-hydraulic code CATHARE, which uses 2 energy balance equations, 2 momentum balance equations, 2 mass balance equations and 2 mass balance equations for 2 non-condensable gases.

- In RATEG/ SVECHA the thermal hydraulic part RATEG uses 7 equations: mass, momentum, and energy equations for each of two-phases and one equation for non-condensables.

- The detailed codes as RELAP/SCDAPSIM, RELAP5/SCDAP (bi9), SCDAP/RELAP5 are based on the thermal-hydraulic code system RELAP5 that uses a 6-equation system and mass balances for non-condensables in the vapor and solutes in the liquid phase.

6.4 Selected Code Options

The computer codes use a set of default parameters. The cladding failure temperature and oxidation correlations are given in Table 7.2.

Cladding failure criteria

In all codes, the cladding failure criterion is a user-defined parameter which strongly influences the progress of the bundle damage, because of the relocation of U-Zr-O melt into the lower/cold part of the core/bundle. From FZK single rod experiments, a certain dependency of the cladding failure temperature on the heat-up rate was observed. This may explain differences in cladding failure temperatures used in the simulation of reactor cores and integral experiments. The cladding failure temperatures are given in column 6 of Table 7.2.

The NRI participant used the value of 2800 K for this criterion, because the default value of 2500 K (default in MELCOR 1.8.6) corresponds to cladding failure as indicated in the Phebus FPT-1 experiment where the cladding-fuel pellet interaction resulted in earlier failure than originally assumed (default in MELCOR 1.8.5 and earlier was 2800 K). And because the QUENCH facility does not use UO_2 fuel pellets, but ZrO_2 as fuel simulator, the NRI participant returned to the original value of 2800 K, which is close to the ZrO_2 melting point. Other participants used the value related to the behavior of a real fuel rod, but he is in the opinion of then not being representative for the QUENCH facility.

Oxidation correlations

The participants used various Zr oxidation correlations which are presented in Table 7.2. For the low temperature regime, they used: Cathcart-Pawel, Leistikov, Leistikov-Schanz, only MELCOR users used Urbanic-Heidrick. In the high-temperature regime the participants used: Urbanic-Heidrick, Prater/Courtright, Leistikov-Aly.

6.5 Modeling of the Test Section

The modeling of the bundle test section by different participants is presented in Table 7.3. The detailed code systems use various mesh lengths in the heated section and in the electrode zones which often include the copper section. Most of the participants simulate the bundle using five components: central unheated rod, inner and outer heated rods, corner rods, and shroud. RUB-LEE and GRS did not simulate the corner rods.

In the following, the basis of the various input decks is outlined.

ICARE/CATHARE

The ICARE/CATHARE V2 calculation by IRSN is based on a fine mesh originated from ENEA studies with ICARE2 developed at IRSN Cadarache to achieve a better representation of the axial temperature profiles prior to reflood. Similar experience was obtained with a 32-nodes input deck used from FZK1.

ASTEC

The FZK 2 input deck originates from an ICARE2 V3mod1 input deck prepared for QUENCH-06 by S. Melis in 2001. During preparation of the experiment QUENCH-11, the

input deck was adapted to new initial conditions. Also, several corrections such as the real length of the corner rods and other improvements were performed to enhance the prediction capability of ASTEC V1.2. Extensions of the online-visualization allowed a faster optimization of experimental parameters.

RELAP/SCDAPSIM

The participants who used RELAP/SCDAPSIM (INR and UZ) relied on an input deck developed by ISS which was distributed as part of the SCDAPSIM package.

MELCOR

The input deck used by INRNE has been developed and validated for the QUENCH-01 experiment. It serves as basis for the input deck of SNL which developed the MELCOR reflood model. For the MELCOR thermal-hydraulic cells a small number of cells are used, but in the bundle simulation a much finer nodalization model was used. The other user (NRI) used a much finer input deck.

ATHLET-CD

The ATHLET-CD input deck from GRS was originally derived from previous CORA calculations and was extended for analyses of various QUENCH experiments. The RUB-LEE input deck has been developed on the basis of the existing QUENCH-01 to QUENCH-09 input decks by implementing the initial and boundary conditions of the QUENCH-11 test as well as the auxiliary heater and water feeding into the lower plenum.

Table 7.3: Modeling of the QUENCH-11 bundle test section by the participants.

Code	Token	Nodalization		Simulated Length [m]	Remarks
		Axial nodes: total/heated	Compo-nents		external Rv, mΩ
SCDAP/ RELAP5	FZK1	32 / 20	7	-0.45 …1.5	4.2
ASTEC	FZK2	21 / 11	6	-0.47 …1.5	4.1
MELCOR 1.8.5	INRNE	22 / 16	4	-0.475 …1.5	4.5
ATHLET-CD 2.1A	GRS	20 / 10	4	-0.475 …1.5	2.0
RATEG/ SVECHA	IBRAE	18 / 10	7	-0.475 …1.5	4.0
MELCOR 1.8.6	NRI	30 / 21	4	-0.47 …1.63	6.5 [1])
ATHLET-CD 2.1A	RUB-LEE	20 / 10	4	-0.475 …1.5	3.0
ICARE/CATHARE	IRSN	35 / 21	5	-0.47 …1.5	4.04
RELAP/SCDAPSIM	UZ	16 / 10	5	-0.475 …1.5	4.0
RELAP/ SCDAPSIM	INR	20 /	5	-0.475 …1.5	

[1)] This value was changed to 4.5 mΩ at 5200 s.

RATEG / SVECHA

The RATEG/SVECHA input deck from IBRAE has been verified for QUENCH-09 and -10. During preparation of the experiment QUENCH-11, the input deck was adjusted to the new initial conditions. The axial model of the bundle included ten cells (see Table 7.3).

SCDAP/RELAP5

The analytical work for the QUENCH program at FZK dates back to the construction of the test facility; the first input deck has been developed at that time. Since the first QUENCH test, calculations have been made for all tests with the same model of the facility, including the calibration of open parameters.

7 Challenges and Limitations of the Benchmark

The benchmark is governed by a number of features [13] that determine the quality and reliability of calculated results and therefore explain their bandwidth at least partly.

The experimental facility is complex with respect to its geometry and so is the experiment. Since the test section is partially filled with water and partially with steam, the axial temperature profile is even more complex than in former QUENCH tests. Also in contrast to former QUENCH tests, the physical conditions in the lower plenum are important for the test conduct.

Establishing stationary boiling at a low evaporation rate means that the system is close to the transition to single-phase flow conditions. This entails a large sensitivity of the system, when other parameters are changed. For such conditions, the power balance with electrical rod and auxiliary power and chemical power input on the one side and convective heat removal and radial heat losses on the other side is a challenging issue.

Direct electric heating of the test rods implies a general problem due the positive feedback of electrical heaters: If the temperature is overestimated at a given location, calculated electrical power input at that location is overestimated, too. Since the total electrical power input is given, electrical power release in other regions is underestimated. At higher temperatures, this sensitivity is further increased because of oxidation increasing local temperature substantially in the hot region. During the test, the axial temperature profile changes substantially with time due to evaporation, and the evaporation rate is partially determined by local electrical power release in the rods, resulting in further feedback, one for the location of the water level, one for convective heat removal above the water.

Accuracy of experimental data, e.g. of thermocouples, is limited as described in section 5. Besides, there are experimental uncertainties beyond accuracy of measuring devices, e.g. high-temperature thermocouples are not appropriate for temperatures below 500 K as at the start of the test. For this reason, the initial axial temperature profile, given in the specification report [4], is provided with a considerably higher uncertainty in the upper half of the bundle compared to the consecutive time when temperatures are above 500 K. The initial temperature distribution is important for any calculation. In particular, it determines the time to heat up the water inventory to saturation temperature, hence the time from the start of the

test to the start of evaporation in QUENCH-11. Finally, important information necessary for reliable calculations as the portion of the electrical rod power that is released into the bundle or the heat losses in the lower plenum was unknown at the start of the benchmark. After the benchmark, various contributions of the heat losses in the lower plenum were assessed (see section 10). FZK/IRS work for this benchmark showed that not even the temperature escalation before quench initiation is calculated in all cases, when input parameters are varied within experimental certainty [13].

Shroud failure during the quench phase of the experiment has a number of consequences. An unknown amount of steam is diverted into the annulus between shroud and inner cooling jacket in spite of the argon flow from that annulus into the bundle that is intended to suppress this lateral steam flow. The proof that this steam flow exists nevertheless is oxidation of the outer shroud surface, seen in post-test analysis. Since temperature in the annulus is lower than in the bundle, the steam cools down and decreases pressure in the annulus, giving rise to a continuation of this lateral steam flow. Increase of the breach region changes the steam mass flow rate additionally. This consequence of shroud failure is aggravated significantly, when the steam condenses in the cold parts of the annulus and in this way increases pressure differences. Condensation does not only occur at the surface of the inner cooling jacket, but also in the very porous ZrO_2 fiber insulation material. None of these effects can be modeled in severe accident codes.

Severe accident codes are devised for analyses of reactors, and need to be verified on the basis of integral experiments. On the other hand, experiments like QUENCH-11 are very complicated and contain some features that are irrelevant for reactors. In particular, important details of geometry and test conditions including the shroud and its failure challenge or even exceed the modeling capabilities. As is well-known from other benchmarks, the skill of the code user to model a test and his understanding of the code play an important role for the quality of the results.

8 Results Delivered by the Participants

The comparison of the participants' results with the experimental data is presented in this section. The calculations were performed up to 7000 s by all participants. Only the FZK 1 results are only given until 6140 s because of a program error. This error also occurred in calculations for other QUENCH tests during the quench phase and has been reported to the code developers. INR calculation results are given up to 5500 s. Not all participants delivered all required data. It was not always possible to clarify questions which arose during data evaluation.

Maximal bundle temperature

The maximum bundle temperature is presented in Figure 9.1. The results of the participants are similar to the trend of experimental data where the maximum temperature corresponds to 950 mm elevation (see also axial temperature profiles). The peak of the participants' maximum bundle temperature is observed between 5600 and 5790 s, if one neglects two spikes in the INR results. The INR results have some deviation during the test at approximately 4200 s up to 5500 s. Taking into account further results like hydrogen

production it seems that the input is not consistent with the experimental conduct, but unfortunately, no further information can be given. The calculated maximum bundle temperatures vary within a range of 300 K.

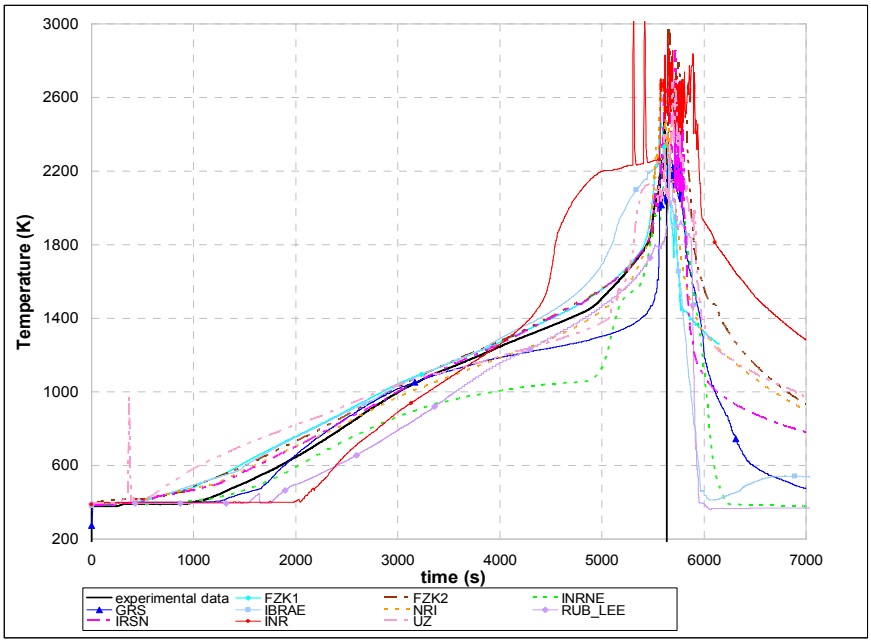

Figure 9.1: Maximal bundle temperature.

The main deviations between calculated and measured maximum bundle temperatures during the transient are observed at around 5000 s, as well as after the quench phase. Among others, the start of the calculated temperature rise above the saturation value depends on the prescribed initial fluid temperature and hence on the time that is needed to reach saturation conditions. This may at least partly explain the scatter between the various calculated data.

Another reason for this scatter is the drawback that the electrical power, released into the bundle, is unknown. Instead, the total electrical power and the external resistance must be used involving some uncertainty in the calculations. The other significant reason for the observed discrepancy (as pointed out above) is the uncertainty in the evaluation of the heat loss. All these uncertainties together with user effects and some code limitations result in significant deviation in the prediction of the heat-up start. Additionally, the beginning of heat-up is also strongly influenced by the corresponding calculated water level which in turn is significantly affected by the correct modeling of the heat balance and the axial profile of the linear electrical rod power as outlined below.

When the calculated start of temperature increase is compared with the measured data, caution is necessary: It is well known that thermocouples, mounted at the outer rod surface, show local effects as e.g. deposition of droplets at their tips which is not modeled in severe accident codes. In the present test, this observation is verified by the scatter in time, when the temperature rise starts.

During the second phase, when the bundle is empty, the behavior of the maximum bundle temperature can be divided into two parts. During the first part, which corresponds to a most comprehensive bundle heat-up with a rate of 0.7 K/s, the participants' results are within a

band of approx. -150 and +150 K. During the second part of this phase, e.g. at 5000 s, the results of most participants are within the mainstream results. It is also observed in the results of two participants that deviations rise above approx. 500 K at that time and continue up to the quench phase. During the second part of the second phase these deviations are additionally observed. In 70 % of the participants' results, the temperature rise rate is not reduced and even increases significantly in one participant's result.

During the quench phase the maximum temperatures reached are in good agreement with the experimental data for the mainstream of results, and this in a significantly narrow range of approx. 200 s compared to the range for start of the transient heat-up. On the other hand, during the final part of the quench phase, or after stopping the quench water flow, a large discrepancy between predicted temperature and experimental data is observed. It is difficult to define a mainstream as the participants' results lie in a fairly wide range, with an upper bound of approx. +800 K and a lower bound of -500 K at 6300 s. The observed discrepancy could be explained with the behavior of collapsed water level in the bundle at that time which is presented in Figures 9.6 and 9.7.

The reason for the discrepancy is that the shroud failed at about 800 mm during the quench phase and some water may have left the bundle through a breach in the shroud. However, the participants did not model this or had no code options to model a failure of the shroud. For ATHLET-CD as an example, it is not possible to calculate the shroud failure due to melting. 60 % of the participants calculated a higher water level.

Cladding temperature of heated rods at +150 mm elevation

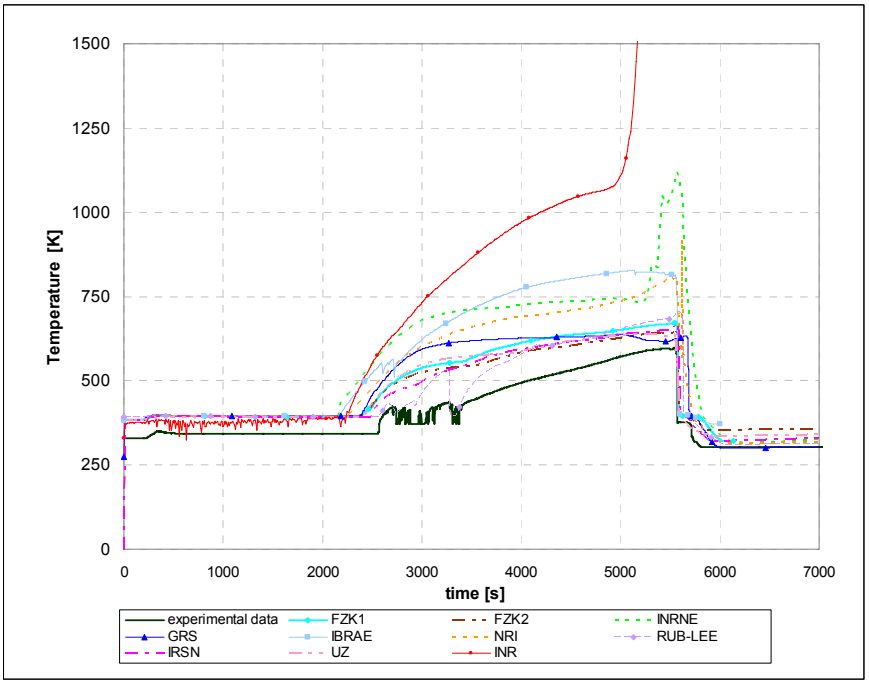

Figure 9.2: Cladding temperature of heated rods at 150 mm elevation.

The cladding temperature at 150 mm is presented in Figure 9.2. The behavior of the calculated cladding temperature at 150 mm is similar to the trend of experimental data, except for the INR result. The mainstream of results during the whole transient varies in a

range of +300 K. The start of the heat-up phase cannot be compared with the measured data as was explained above. During the second phase, the calculated results are in a range of approx. +300 K. During the second part of this phase, the results of only one participant exceeded the experimental data for more than + 300 K (at 5000 s and continuously up to the quench phase).

During the quench phase the calculated temperatures are in good agreement with experimental data within the mainstream of results being in the range of approx. 200 K compared to the experimental data. The discrepancy could be explained with the behavior of collapsed water level in the bundle.

Cladding temperature of heated rods at +550 mm

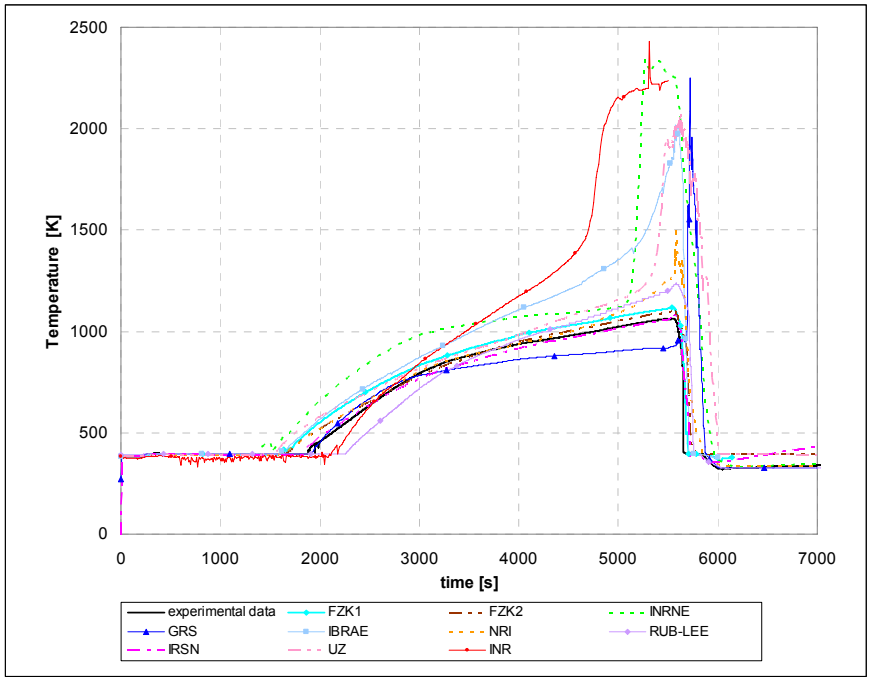

Figure 9.3: Cladding temperature of heated rods at 550 mm elevation.

The comparison of the calculated cladding temperature at 550 mm with the experimental data is presented in Figure 9.3. As can be seen from the figure, 50 % of the participants' results are in very good agreement with the experimental data except for the calculations of INRNE, INR, IBRAE, UZ and GRS. During the second phase, 50 % of the participants' results vary in the range of approx. ±50 K while the other part of the participants predicted the cladding temperature to lie within +100 K. The peak in the cladding temperature at 550 mm predicted by the participants lies between 5270 and 5720 s, i.e. before and during the quench phase. 50 % of the participants predicted a very good agreement with the experimental data while the other part of the participants predicted significantly higher temperatures (approx. +1000 K) compared to the experimental data. After the quench phase the mainstream of the participants' results are in good agreement with experimental data (approx. 50 K).

Cladding temperature of heated rods at +1150 mm

The cladding temperature at 1150 mm predicted by the participants in comparison to the experimental data is given in Figure 9.4.

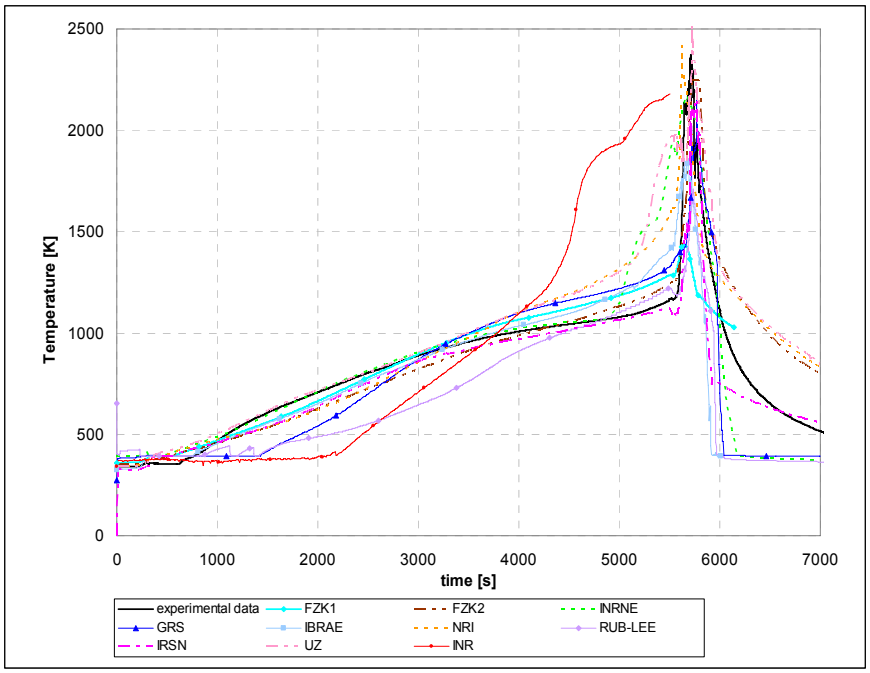

Figure 9.4: Cladding temperature of heated rods at 1150 mm elevation.

As can be seen from the figure the mainstream of results is in good agreement with the experimental data except for one calculation. During the second phase, code predictions of the cladding temperature are in a range of approx. ±250 K compared to the experimental data. The peak of the cladding temperature at 1150 mm predicted by the participants lies between 5620 and 5720 s, i.e. in the quench phase. The participants' predictions are in fair agreement with the experimental data, i.e. in a range of approx. ±500 K, except for IRSN exceeding this range. The observed discrepancy could be explained with behavior of the collapsed water level in the bundle, different axial bundle modeling and incorrect heat transfer.

Shroud temperature at 950 mm

To compare the measured shroud temperature with the one calculated by the participants, please refer to Figure 9.5. The participants' results are similar to the trend of the experimental data except for one calculation. During the first part of the second phase, when the bundle is empty, most of the participants predict shroud temperatures in the range of approx. ±150 K compared to the experimental data. The calculated and measured maximal shroud temperature is observed at approx. 5620 s. The mainstream of computational results is in the range of approx. ±250 K. In the quench phase or especially after turning off the water injection there is a larger discrepancy of the calculated results compared to the experiment. The reason for such a behavior is that during the quench phase the shroud failed at around 800 mm and it was possible for the injected water to leave the bundle through the opening. There are no code options to model a failure of the shroud, and

therefore 60 % of the participants calculated a higher water level. The sharp temperature decrease to 0 K is a feature of MELCOR to indicate material relocation.

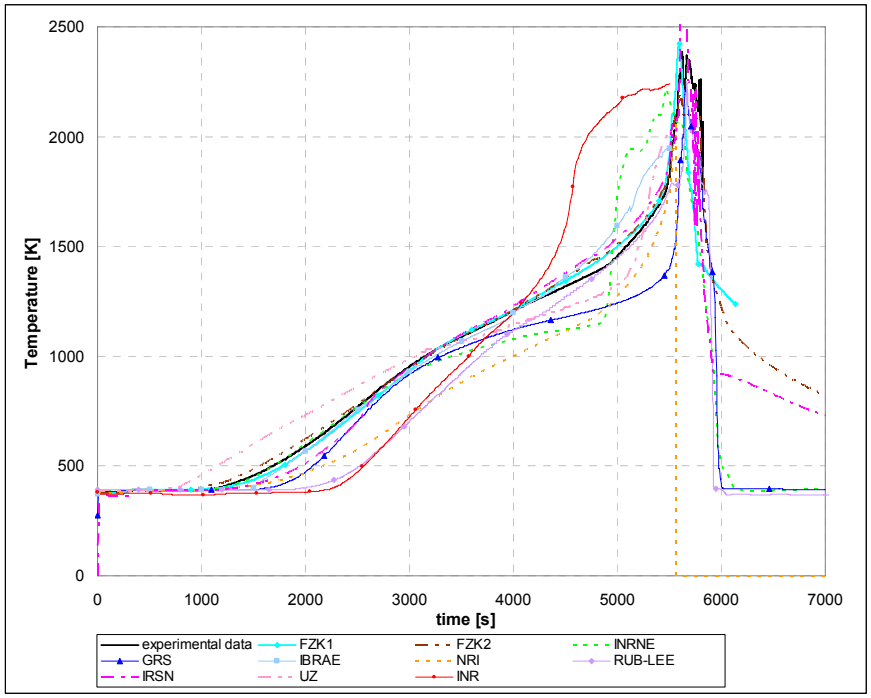

Figure 9.5: Shroud temperature at 950 mm elevation.

Collapsed water level during boil-off and reflood phase

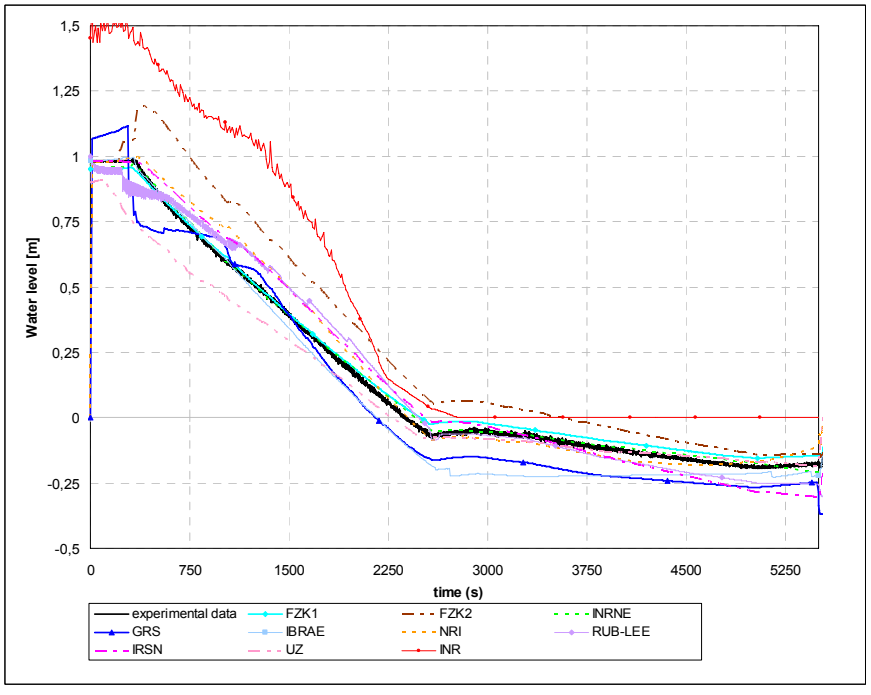

Figure 9.6: **Collapsed water level during the boil-off phase, i.e. in the time period of 0-5500 s.**

The comparison of measured and calculated collapsed water level in the bundle is presented in Figures 9.6 and 9.7. The mainstream of the delivered results closely follows the experimental data in the first and second phase as well as in the first part of the third phase. There is only one calculation for the collapsed water level that starts at 1.5 m instead of 0.98 m and predicts a reduction in the water level significantly faster compared to the others. The scatter, when the evaporation starts (decrease of water level early in the test), is by far smaller than for the increase of the maximum bundle temperature.

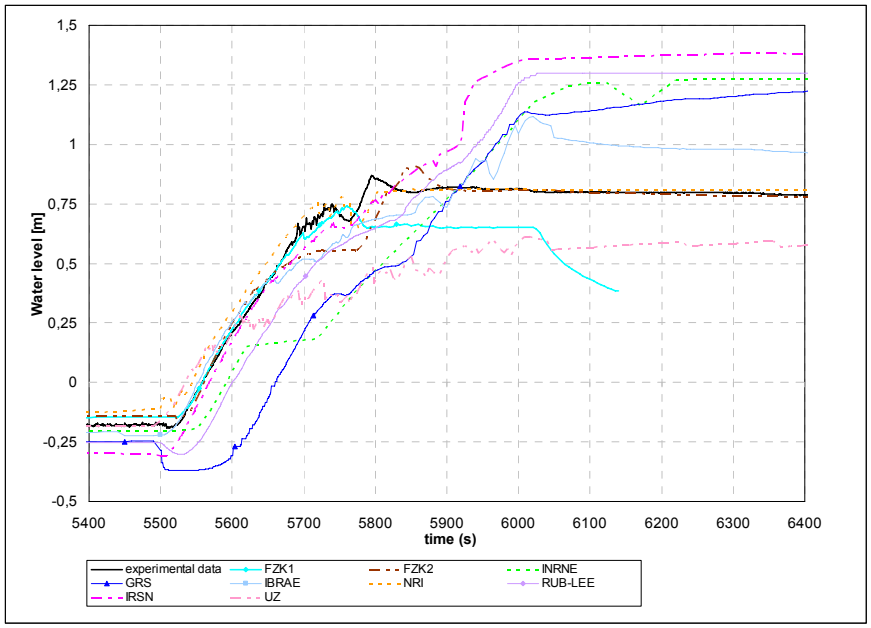

Figure 9.7: **Collapsed water level during the quenching phase, i.e. in the time period of 5400-6400 s.**

At the end of the reflood/quench phase the participants predict the collapsed water level within a significantly large range, i.e. within a lower bound of 0.386 m and an upper bound of 1.38 m. The possible reason for such a behavior is pointed out above. There is one calculation in which (after the beginning of quenching) the water level continues for some short period of time to drop down to bundle level -0.37 m. During the second stage of the quench phase most calculations are slightly below the experimental curve.

Steam flow rates during boil-off, transient and reflood phase

The calculated steam flow rates which refer to the bundle outlet are presented in Figures 9.8 and 9.9. A correct prediction of steam flow rates directly reflects the quality of hydrogen generation as well as the distribution of the axial temperature profile.

The experimental data are based on L 501 and L 701 readings as well as the steam measurement by mass spectrometry. In particular, data derived from L 501, refer to the evaporation rate whereas mass spectrometer and L 701 (differentiated) data refer to the steam mass flow at the bundle outlet under the assumption that no condensation occurs afterwards. The difference between the two sets of data is the steam consumption by oxidation.

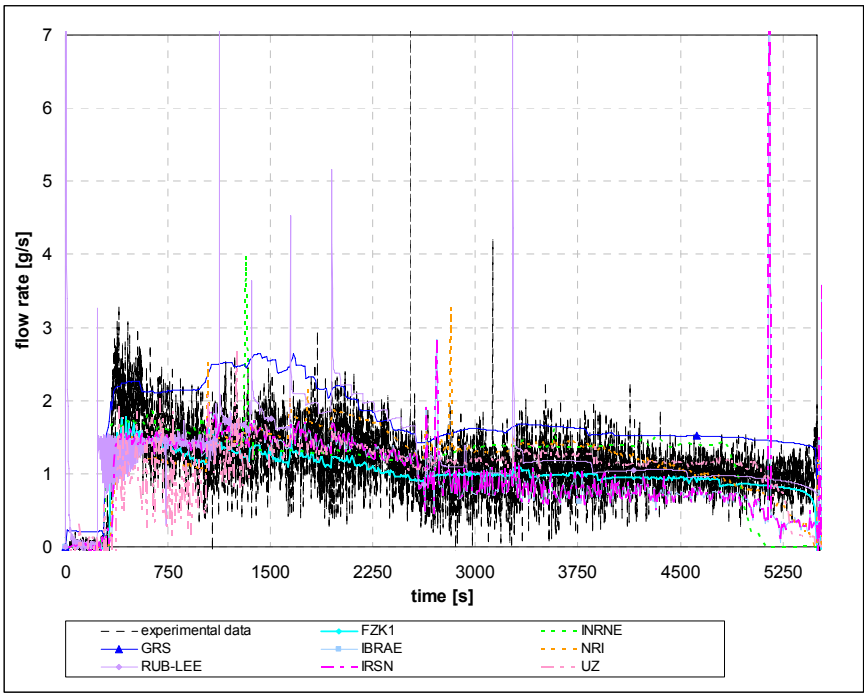

Figure 9.8: Steam flow rate for the time period of 0-5500 s.

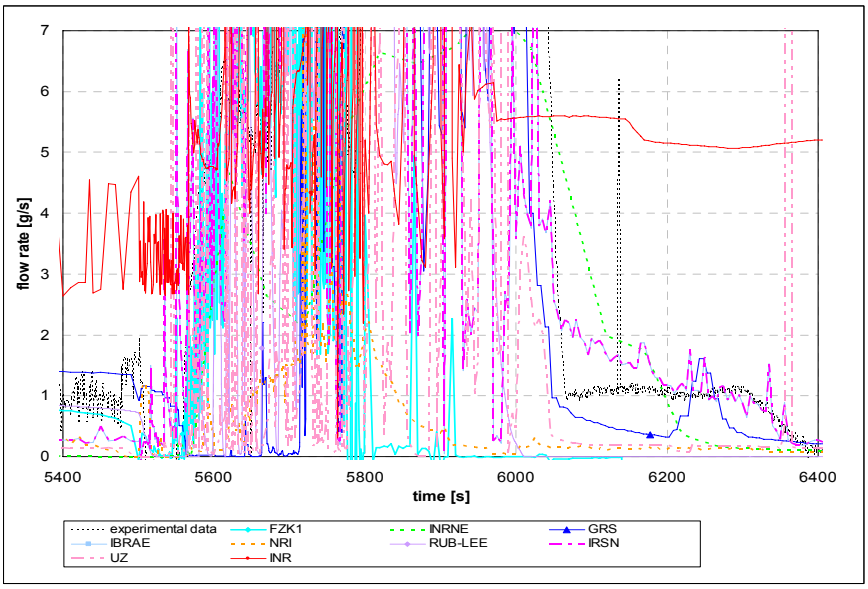

Figure 9.9: Steam flow rate for the time period of 5400-6000 s.

The evaporation rate until 2200 s depends on the bundle power and after that time, the evaporation rate depends mainly on the auxiliary water injection and the power of the auxiliary heater (see Figure 9.8). This is true until the quench phase. In this way, usage of an auxiliary heater made it possible to avoid steam starvation in the bundle and allow an effective control of the water level in the bundle during the transient heat-up phase. One of the reasons to control the evaporation rate is to achieve a quasi-stationary steam flow rate.

The experimental data are smoothed to decrease noise. In particular, data derived from L 501, refer to the evaporation rate whereas mass spectrometer and L 701 (differentiated) data refer to the steam mass flow at the bundle outlet under the assumption that no

condensation occurs afterwards. The difference between the two sets of data is the steam consumption by oxidation.

The mainstream of the delivered results, which included all except one, predict steam flow rate in the range of 1 to 2 g/s starting from 300 to approximately 5000 s.

After that time the steam flow rate is reduced due to a larger consumption (see Figure 9.8). Calculations demonstrate a rapid increase in steam generation during quenching. After an increase in the water level, steam flow rates are reduced to very low levels (almost zero for some participants). The INR calculations on steam generation are not presented in Figure 9.8 because of extremely strong fluctuations that cover the results of the other participants. The INR results are not within the mainstream of the results which could be due to inappropriate simulation of the auxiliary heater. The GRS calculations over-predict the steam flow rate to some 20 % compared to the mainstream results which can be considered as acceptable.

Figure 9.9 shows strong fluctuations in the steam flow rates during the quench phase for almost all delivered computational results. In this figure the INR results are included. The calculated hydrogen generation rates result in the same fluctuations. The reason for such fluctuations may be explained by condensation processes.

Hydrogen generation rate

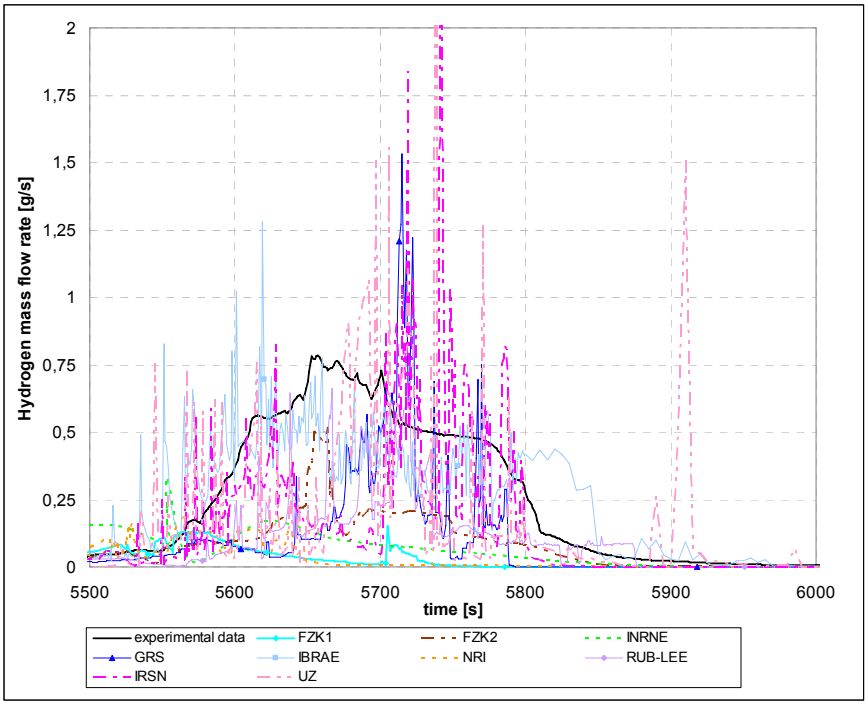

Figure 9.10: Hydrogen production rate.

The participants' calculated hydrogen generation rates at 5500-6000 s are presented in Figure 9.10. There are some deviations between calculated and experimental data depending on the code ability and the participant's approach to model the test. Experimental data show smooth data in the hydrogen rate, i.e. smooth increase for 0.6 g/s at approximately 5600 s and some stable value of 0.5-0.7 g/s, until 5780 s, followed by a

smooth decrease at approximately 5800 s. Most calculations predict some fluctuations, especially the INR results which were taken out of Figure 9.10 to avoid covering the other results. The fluctuations are caused by the oscillating oxidation reaction due to the steam consumption process. The calculated thermal behavior significantly influences the hydrogen generation as well.

In contrast to the experimental data within this time period, some calculations predict significantly lower values which result in lower integral values.

Total hydrogen generation

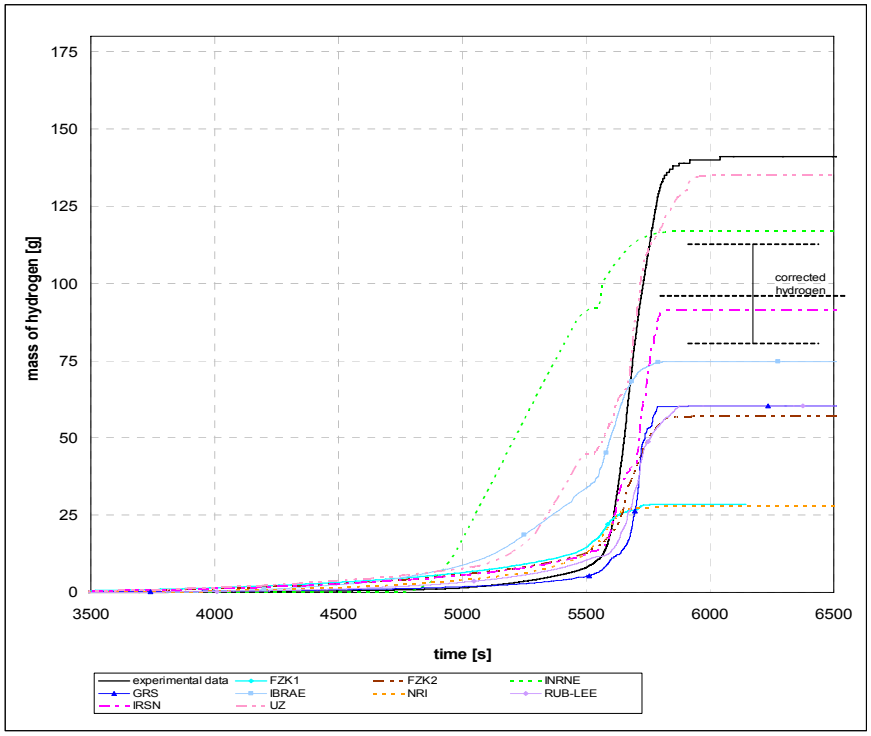

Figure 9.11: Total hydrogen production during the QUENCH-11 experiment.

The participants' results on total hydrogen generation are plotted in Figure 9.11 for the time period of 3500-6500 s. The hydrogen produced by non-prototypical materials has to be taken into account for the measured data. In Figure 9.11, however, the total mass of hydrogen generation of 141 g is presented, including hydrogen produced by non-prototypical materials. The hydrogen mass produced by the prototypical materials amounts to 92 g, with an uncertainty of approx. 20 %. Cladding oxidation was detected in the experiment at 4900 s, when the maximal bundle temperature was approximately 1160 K. The mainstream of the results, which include 80 % of participants' results, predict a total hydrogen mass generation in the band of min 60 g to max 135 g. The INR prediction with a maximum of 450 g hydrogen is an unrealistic value.

The minimum of 29 g is far below the accepted lower bound of hydrogen. The participant supposes, however, that further tuning within accepted uncertainties would lead to better results. The steeper increase of total hydrogen production after about 5000 s, some participants calculated, is only possible, when they calculate a higher evaporation rate. Since

the calculated collapsed water level is more or less constant (Figure 9.6), it seems that the auxiliary water feed is overestimated.

In the NRI calculation a small amount of hydrogen production was observed due to low hold up of molten Zr by ZrO_2 shell, very fast downward progression (candling) of molten Zr, practical absence of melt oxidation (negligible contribution of melt oxidation to total hydrogen generation), and a collapse of all parts of the shroud above elevation 850 mm and relocation of this material. The underestimation of hydrogen can be explained with the shroud failure during quenching and with the history up to quench initiation.

In this way, filling the bundle to only 800 mm and producing a huge volume of steam at that moment could result in intensified oxidation, especially in the upper part of the bundle. In the experiment more than 90 % of hydrogen was produced between 5600 and 5830 s. This is reproduced by the mainstream of the results. After 5600 s the observed maximal bundle temperature is above 1800 K in the experiment and calculations. At that time, all presented calculations predict maximal bundle temperatures to lie above 1800 K, and most of the hydrogen is calculated and measured to be released at that time.

Axial distribution of linear power per rod

The comparison of the calculated axial distribution of linear power is shown in Figure 9.12. The comparison is performed for the start of the quench phase. The exothermal heat increases the local rod temperature and hence the electrical resistance of the tungsten heater, which increases the local heating power. The mainstream data are very close together, except for two participants. The maximum power is reached at 0.95 m. The INR results deviate strongly from the other results for the axial distribution of the linear power profile, particularly for the heated zone.

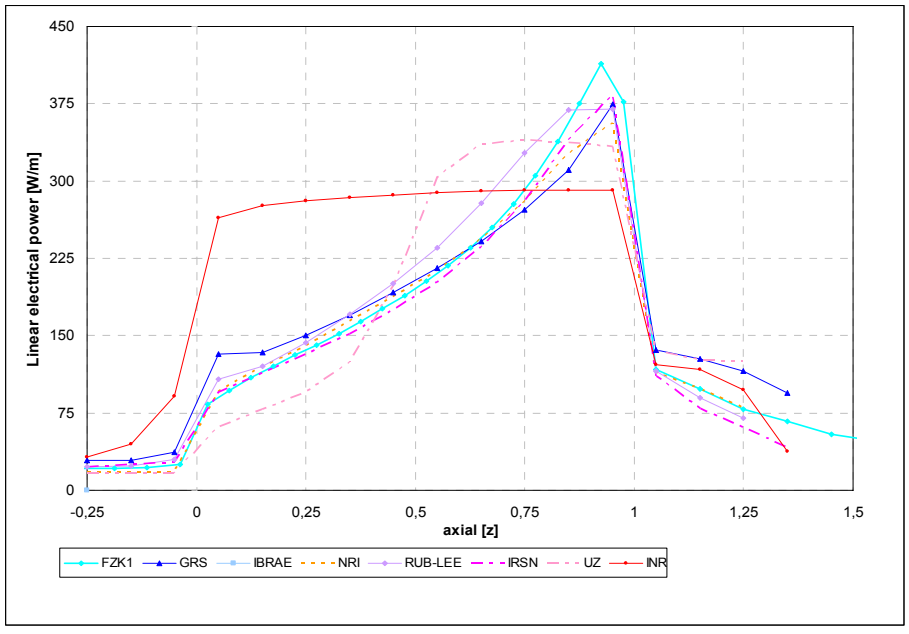

Figure 9.12: Axial distribution of linear electrical power per rod.

Axial distribution of fluid flow area for the final state

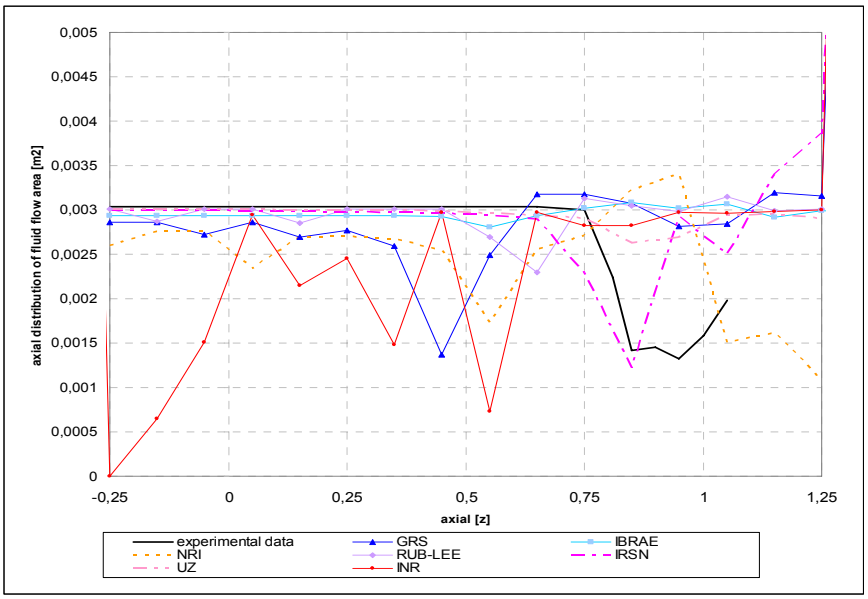

Figure 9.13: Axial distribution of fluid flow area for the final state (at 7000 s).

The comparison of experimental and calculated data on axial distribution of fluid flow area for the final state is presented in Figure 9.13. In this figure the experimental data ("data 1" listed in Table 6.3) are based on a deliberately unchanged inner shroud diameter of 80 mm and are meant to be compared with the results of those participants who did not calculate shroud failure. In contrast, experimental "data 2" of Table 6.3, which are not depicted in Figure 9.13, are based on the real inner shroud diameter and could be taken for comparison with results of those codes able to model shroud and its deformation and failure. The computational results given in Figure 9.13 demonstrate some deviations. Assuming that all participants used the same water injection rate with the same water temperature of 20 ˚C, the deviations could e.g. be explained by differences in the axial power distribution of the bundle.

Axial temperature profile of the bundle at 5490 s (before quenching)

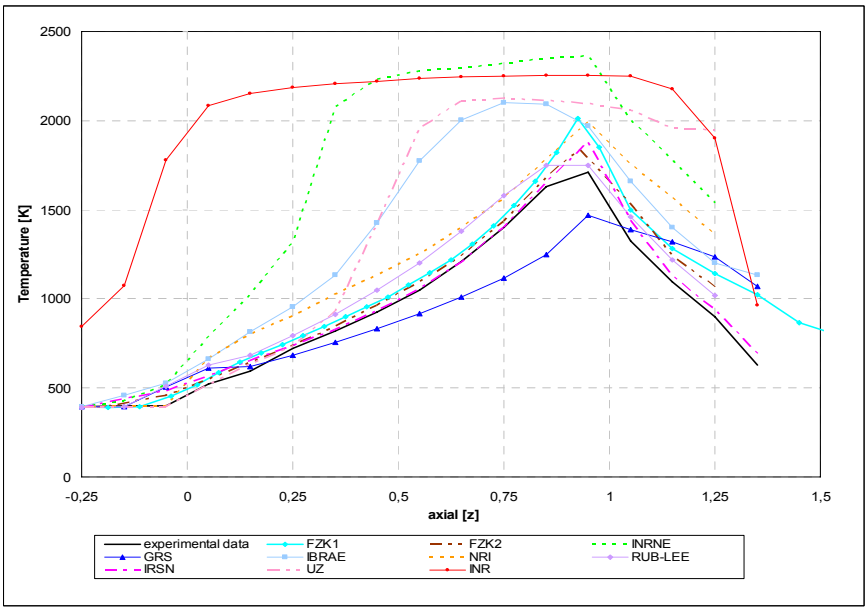

Figure 9.14: Axial temperature profile of the bundle at 5490 s (before quenching).

The axial temperature profile of the bundle at 5490 s (before quenching) is presented in Figure 9.14. The results presented in this figure show that 60 % of the participants predict similar characteristics of the axial temperature profile of the bundle before quenching compared to the trend of experimental data with a peak value at 950 mm elevation. The same percentage of participants predicts the peak values at the level of 0.9 m. For the other 40 % of the calculated results there are deviations from the experimental data with different magnitudes. The deviations in these calculations can be explained with differences in the steam flow generation rate just before quench initiation as well as with the hydrogen generation which started in all four calculations earlier compared to the others and the experimental data. Investigating two of the results with larger deviation in more detail it is seen that the results of INRNE at 5490 s lack a steam flow (probably completely consumed), whereas there is abundant steam at that time in the INR results. Generated (chemical) power from the oxidation in the INR calculation as well as in other calculations delivered by INRNE, UZ and IBRAE causes deviations in the axial temperature profile compared to experimental data. The axial temperature profile of the INR calculation could not be improved although sufficient steam was available.

Comparison of the delivered results on the axial temperature profile of the bundle at 5490 s (before quenching) with the experimental data shows that 90 % over-predict the peak temperature by some 250-300 K, and there is only one set of results that under-predict it with around 200 K. So, the mainstream of calculated maximum bundle temperatures varies in the range of 300 K. The main deviation between mainstream and experimental data is at 0.9 m (axial level of peak temperature).

Axial temperature profile of the bundle at 7000 s (final state)

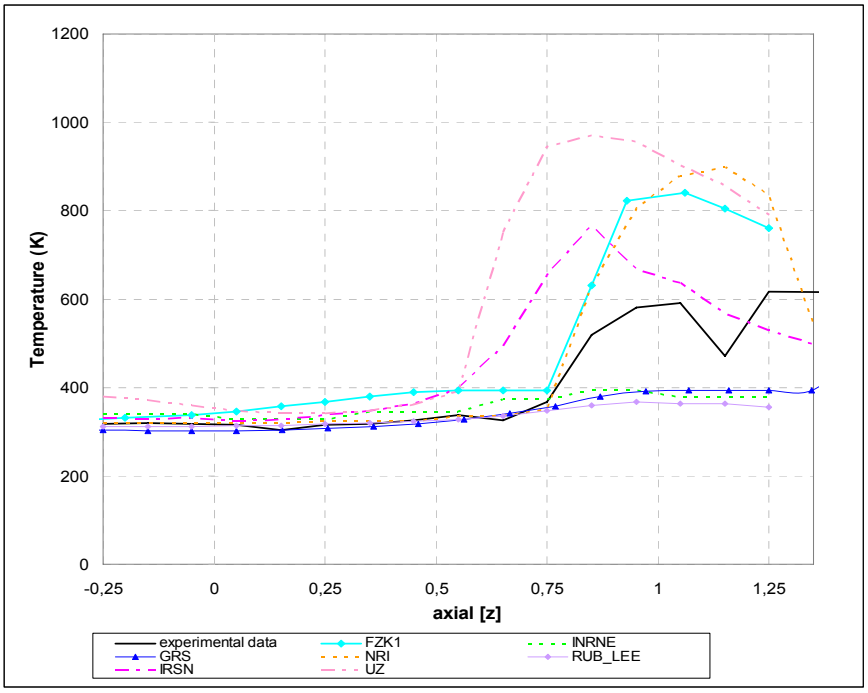

Figure 9.15: Axial temperature profile of the bundle at 7000 s (final state).

The axial temperature profile of the bundle at the final state (7000 s) is presented in Figure 9.15. At this time the test bundle is filled with water from the bottom to above the

0.5-m level. As can be seen from the figure 100 % of the participants have predicted the same trend compared with the measured data. This agreement is best up to 0.25 m elevation and varies more above this level compared to the measured data. The explanation of such kind of deviations is due to the prediction of the significantly different bundle water level and hence to the cooling of the bundle which is among others clearly influenced by the shroud failure being incalculable with the codes.

Axial shroud temperature at 5490 s

Axial shroud temperature at quench initiation is presented in Figure 9.16. The presented results are calculated for 5490 s.

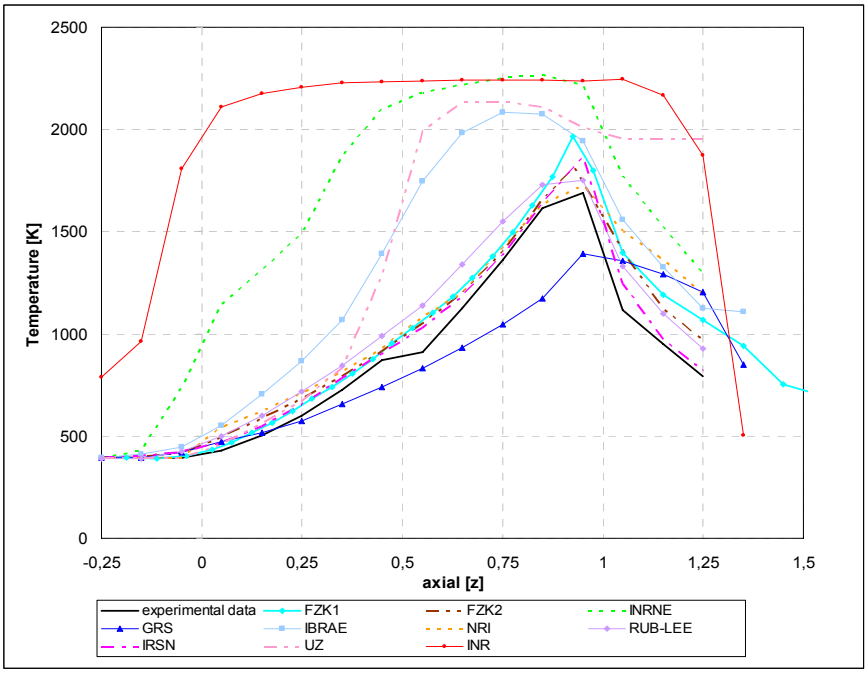

Figure 9.16: Axial shroud temperature at 5490 s (before quenching).

As shown in Figure 9.16 there are 50 % of the participants presenting a very similar distribution of axial temperature. The other 50 % of the participants predict significantly different distributions of the axial shroud temperature. The explanation for such a kind of deviation from the mainstream may be a significantly different bundle water level at that time as well as a different axial power distribution.

Axial shroud temperature at 7000 s

The axial shroud temperature profile at the end of the quench phase is presented in Figure 9.17. The presented results are calculated for the time of 7000 s. As shown in this figure, from 0 to 0.5 m elevation almost 100 % of the calculated curves have a very similar distribution of the axial shroud temperature. The reason for such an agreement is that at that time the bundle section is filled with water at least to the 0.5 m elevation. Above mid-plane, the participants predict significantly different distributions of the axial shroud temperature due to different predictions of the bundle water level at that time.

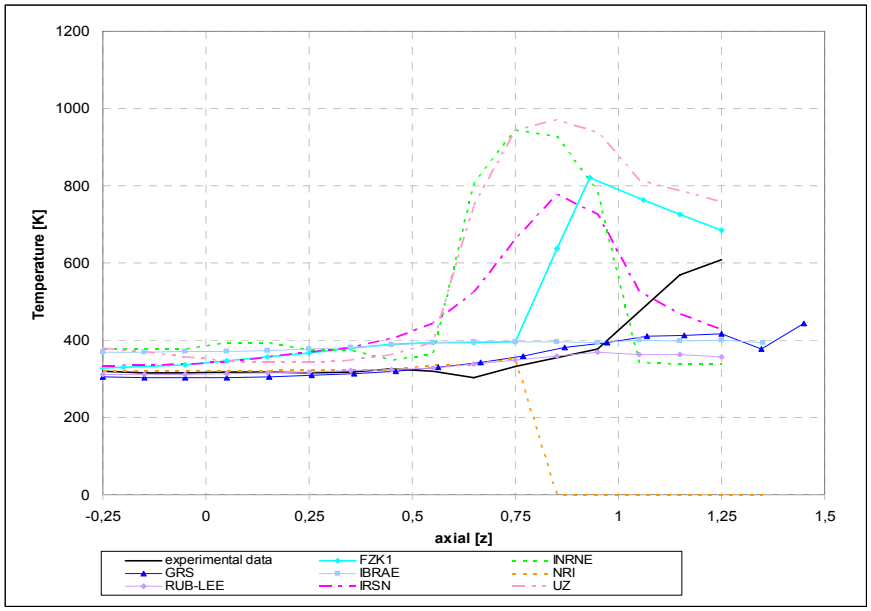

Figure 9.17: Axial shroud temperature at 7000 s (final state).

Axial distribution of oxide layer thickness at 7000 s

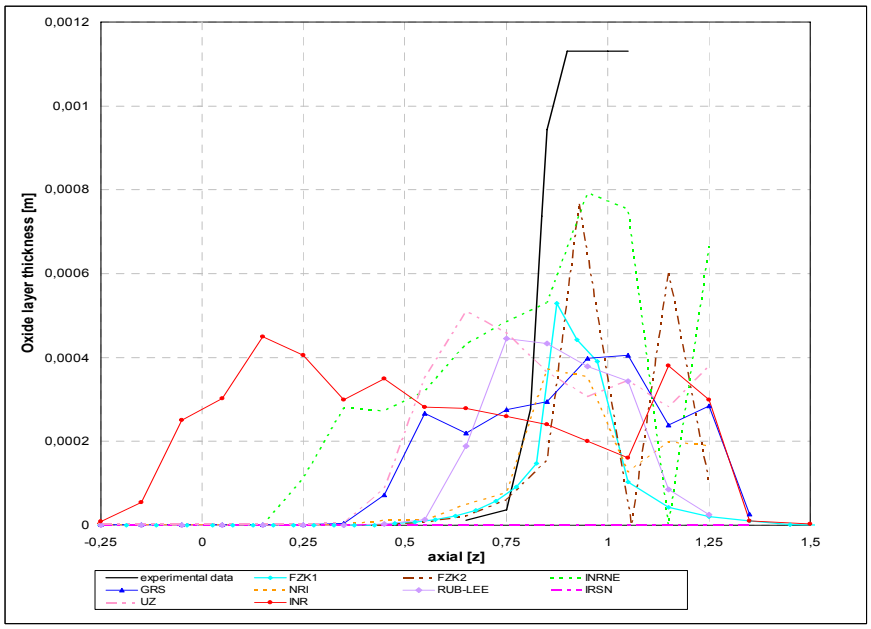

Figure 9:18: Axial distribution of oxide layer at 7000 s (final state).

The axial distribution of the oxide layer thickness for the final bundle state, i.e. at 7000 s, is presented in Figure 9.18. The computational results in this figure show a significantly different axial distribution of the oxide layer compared to the experimental data. As it is evident from this figure, it is difficult to establish a mainstream of results. There are not two curves with similar trends. The peak cladding oxidation is at the level of approx. 0.9 m for just three participants, while all other participants predict peak oxidations in a significantly wide range starting from 0.25 m up to level 1.15 m. Reasons for such discrepancies could be incorrect calculated axial power distributions or heat losses at the bottom of the QUENCH test section. This latter uncertainty causes incorrect water levels in the bundle at the time e.g. just before quenching.

Final axial distribution of debris, Zry and ZrO_2 (at 7000 s)

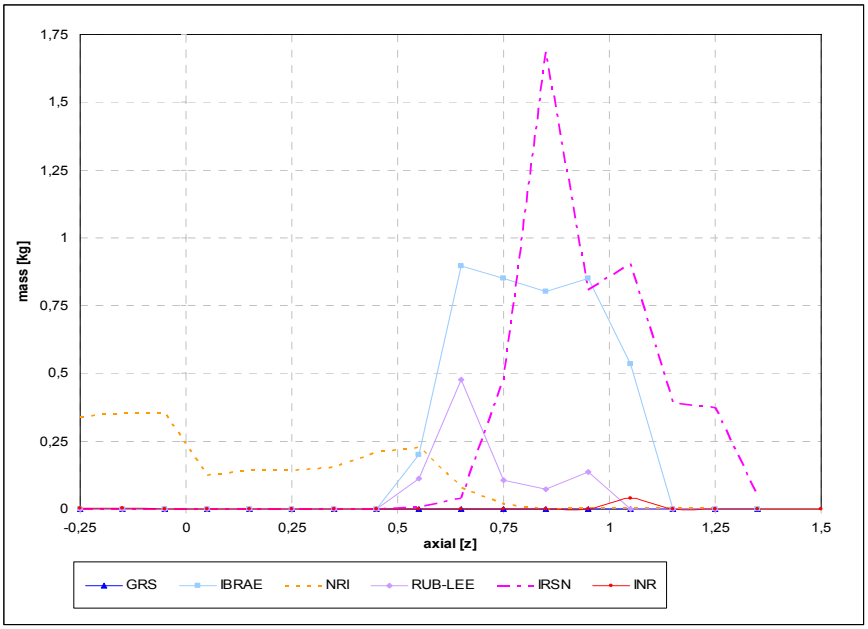

Figure 9.19: Final axial distribution of debris (at 7000 s).

The final distributions of debris, Zircaloy and ZrO_2 (at 7000 s) are presented in the following Figures 9.19-9.21.

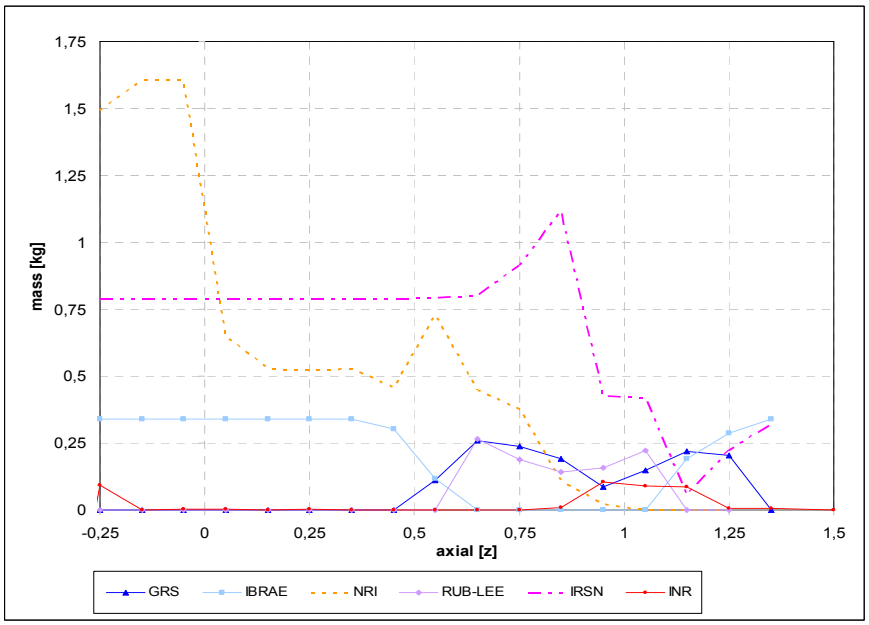

Figure 9.20: Final axial distribution of Zircaloy (at 7000 s).

As can be seen from the figures the participants predicted significantly different axial distributions in the categories debris, Zircaloy and ZrO_2. Most of the participants predicted the start of material relocation to be at 0.5 m elevation. Other participants predicted the start of material relocation at lower elevations depending on different modeling approaches and failure criteria. Experimental data are evaluated from cross sections and can only be given in

as free flow area (see Table 6.3) and not as mass distribution. So, a direct comparison of experimental and calculated results is not possible.

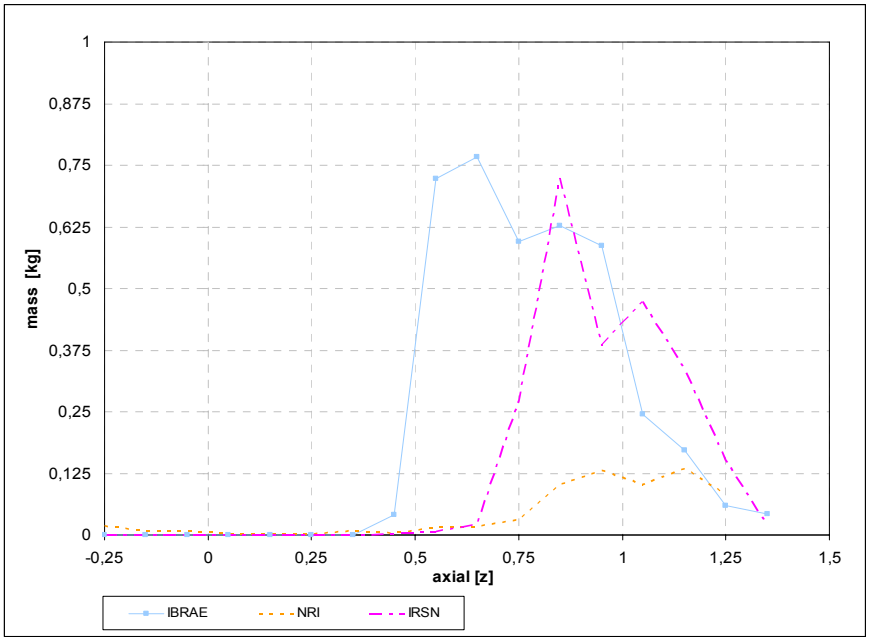

Figure 9.21: Final axial distribution of ZrO_2 (at 7000 s).

In addition, a comparison between the different calculated results is difficult as well because the definitions of the three categories are interpreted inconsistently. For example, IRSN assumed: (1) the debris includes all molten and relocated materials, (2) the Zry mass includes all intact and non-oxidized molten Zry in relocated material mixtures, (3) the ZrO_2 mass includes all intact and relocated ZrO_2 in material mixtures. For the INR and GRS participants debris contains only the portion which corresponds to Zr. The RUB-LEE definition of debris includes the sum of metallic and ceramic melt and crust formation, whereas no ceramic melt and crust is calculated, because the temperature criterion for ceramic melt relocation is set to 3200 K (solidus) considering the simulation of fuel by tungsten heaters and ZrO_2 ring pellets. The understanding and interpretation of the terms "mass of debris, Zry and ZrO_2" by the NRI participant (MELCOR 1.8.6 code) are the following:

- Debris – includes only masses of candled and relocated Zr and ZrO_2
- Zry – includes masses of intact and candled or relocated Zr
- ZrO_2 – includes masses of ZrO_2 in intact position and candled or relocated as well.

The differences in the results for ZrO_2 (Figure 9.21) are smaller due to an overall less amount of ZrO_2 which is localized mainly in the upper part of the bundle.

9 Sensitivity Study of IBRAE Concerning Heat Losses in the Lower Plenum

In our opinion, there are four sources of heat loss from the lower plenum (LP), (see Figure 10.1):

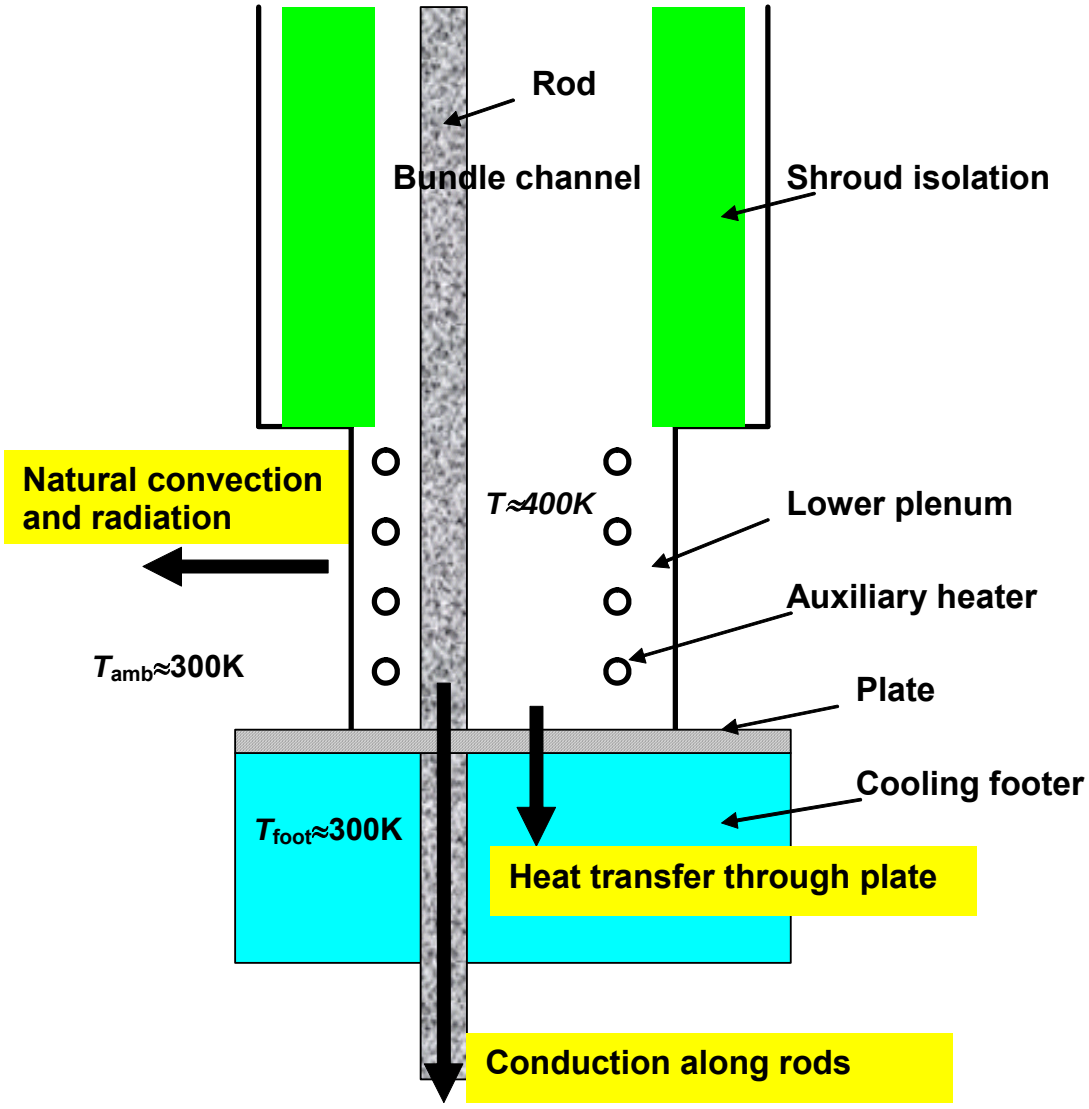

Figure 10.1: Schematic representation of the lower part of the QUENCH test section.

- Heat loss from outer boundary of lower plenum by natural convection and radiation;
- Heat loss via the inlet pipes entering the lower plenum;
- Heat conductivity along the rods to the cooling footer (CF);
- Heat flux from the water in lower plenum to CF through the plate between LP and CF.

Let us estimate these heat losses. Finally, in calculations, of course, one adjusts the total heat losses in the SA code, but assessing the various contributions has its own value and gives by far more insight.

The convective heat transfer between a vertical wall and surrounding gas (air) for turbulent convection (it is our case) is described by Nusselt number [15]:

$$Nu = \frac{hL}{\kappa} = 0.1Ra^{1/3}, \quad (1)$$

where h is the heat transfer coefficient [W/(m^{2}K)], L the characteristic size (wall height) [0.15 m], κ the gas thermal conductivity [0.026 W/(m K)] and Rayleigh number Ra is written as

$$Ra = \frac{g\beta(T_w - T_{amb})L^3}{\nu\chi} \quad (2)$$

Here, g - gravity acceleration [9.8 m/s^2], β the gas volumetric expansion coefficient [3.67·10^{-3} 1/K], T_w the wall outer temperature [K], T_{amb} the surrounding gas (air) temperature [K], $\nu=\mu/\rho$ [1.23·10^{-5} m^2/s] the gas kinematic viscosity, μ the gas dynamic viscosity [1.6·10^{-5} Pa·s], ρ the gas density [1.3 kg/m^3], $\chi=\kappa/c$ the thermal diffusivity [1.96·10^{-5} m^2/s], $c=\rho c_p$ the gas heat capacity of unit volume [J/(m^3 K)], c_p =1020 J/(kg K).

After substitution of thermo-physical properties of air we obtain for heat transfer coefficient:

h=1.4·[T_w-T_{amb}]$^{1/3}$ W/(m^2 K), (3)

The heat flux will be

$$q = h(T_w - T_{amb})S, \quad (4)$$

where S is the heat transfer surface area [5·10^{-2} m^2]. The Rayleigh number is strongly dependent on the characteristic size L and is about 5·10^7 for L=0.15 m.

Finally, we get the estimation of only about 35 W for heat transfer loss due to natural convection because of a small interfacial area.

The radiative heat flux is about

$$q_{rad} = \sigma_B \frac{1}{\left(\frac{1}{\varepsilon_w} + \frac{1}{\varepsilon_{amb}} - 1\right)}\left(T_w^4 - T_{amb}^4\right), \quad (5)$$

where σ_B - Stephan-Boltzmann constant, ε_w and ε_{amb} are emissivity factors of external wall and ambient medium, T_w and T_{amb} are corresponding temperatures. If $T_w \approx$400 K and $T_{amb} \approx$300 K, then $q_{rad} \approx$525 W/m^2 and the integral radiative heat loss from all lower plenum surface (product of heat transfer flux and the area) is of the order of 25÷30 W which is also a sufficiently small value.

The heat losses via inlet pipes are also, in our opinion, several tens of Watts. We can estimate them as thermal conductivity of water (0.68 W/m/K) times the characteristic temperature gradient times the cross-section surface of the tubes.

The heat conduction flux along one heated rod is estimated as product of characteristic thermal conductivity of copper κ_{cu}≈120 W/(m K), the rod cross-section surface area S_{cu}≈6.0·10^{-5} m^2 and the temperature gradient in axial direction $\cdot\Delta T/d_{char}$, where ΔT~100÷200 K and the characteristic axial length d_{char} ~ 0.1 m. Therefore, the total heat conduction flux through all 21 rods will be of the order of 100÷200 W.

Let us make a rough estimation of heat transfer through the plate from the inlet section to the cooling footer which is located beneath the inlet section. If the difference of the water temperature between upper and lower parts of the steel plate is about ΔT=100 K, then for the surface exchange area S_{down}=8.7·10^{-3} m^2 and steel plate thickness d_{steel}=4·10^{-2} m we have the heat flux $q_{down}=\kappa_{steel}\cdot\Delta T\cdot S_{down}/d_{steel}$=435 W. The steel thermal conductivity was estimated to be 20 W/(m K).

Note, that in reality the outer wall of the lower plenum is heated in the QUENCH-11 test to minimize the heat losses to radial direction, but, as we can see from the estimations, these losses are negligible in comparison to the heat loss in the downward direction.

So, for an evaporation rate of 1 g/s water 2.2 kW are needed. About 0.5 W is necessary to compensate the heat losses to the side and bottom. The auxiliary heating power of about 3 kW seems to be reasonable.

The heat losses in the QUENCH lower plenum are important, also for previous QUENCH tests. As long as the lower plenum is at high temperature in those tests, the first constituents of the heat loss are higher for these dry tests without water inventory. Indeed, in that case the temperature difference between the gas mixture in the lower plenum and the ambient medium or the water in the cooling footer is ΔT~300÷400 K, approximately two times larger in comparison to QUENCH-11.

However, the major constituent of the overall heat loss in the case of QUENCH-11 is the last term, namely the heat flux from the water in lower plenum to CF through the plate between LP and CF. In the case of previous QUENCH tests, this term seems to be approximately one order of magnitude lower due to much less dense medium (gas instead of water) resulting to less heat transfer to the plate between LP and CF.

So, in the case of previous QUENCH tests the heat losses may be approximately several times lower than in the present test.

Figure 10.2 presents the RATEG/SVECHA sensitivity study of water level dynamics in dependency of different total heat loss power from the lower plenum. The heat loss value of 750 W seems to be the best approximation for the heat loss value; also, it is in reasonable accordance with analytical estimations made above.

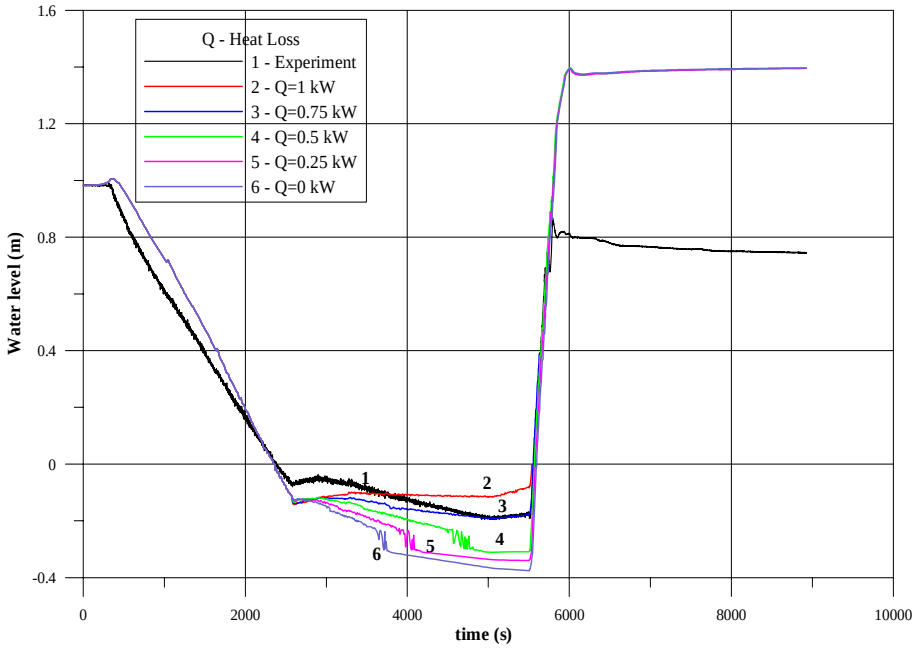

Figure 10.2: Sensitivity study; water level dependence on heat loss.

10 Participants' Conclusions

10.1 Conclusions of the RUB-LEE Participants

1.) In comparison to other QUENCH test calculations more work had to be spent on the reproduction of the thermal-hydraulics of QUENCH-11 as a boil-off experiment with subsequent flooding. Therefore the correct modeling of the auxiliary heat input into the fluid is one of the most important aspects, because heat losses in the lower plenum have to be considered very carefully to predict the characteristics of the water level correctly.

So, RUB-LEE modeled the auxiliary heater as heat conducting structure with an internal heat source. The inner side of this heat conducting element is coupled to the fluid path, whereas the outer side is connected to a boundary condition, which is approx. given by the fluid inlet temperature characteristics(see Ref. [16], [17], [18], [19]).

2.) The external resistance per rod of the heat elements is another important input parameter, which especially influences the reproduction of the thermal behavior. RUB-LEE used a value of 3 mΩ per rod.

3.) The thermal-hydraulics as well as the thermal behavior of the test bundle is predicted very well.

4.) The calculation results are exceptionally influenced by the reproduction of the relocation in the upper part of the bundle and the oxidation rate correlation.

The best calculation results concerning the zirconium oxidation are simulated using the correlations of Leistikow (< 1800 K) and Prater/Courtright (> 2600 K) with an interpolation range between them.

Additionally, the (melt) candling velocity is reduced to 5 mm/s to be able to predict the material relocation in the bundle correctly.

5.) The reproduction of the 9 g of hydrogen generation before the onset of quenching is calculated qualitatively and quantitatively very well within the RUB-LEE simulation, whereas the H_2 generation is under-estimated during the reflood phase leading to an under-prediction of the total amount of hydrogen. Compared with the measured hydrogen production due to the oxidation of the modeled components (119 g for RUB-LEE), the global under-prediction amounts to 49 % in the calculation (see Ref. [11], [17],[18],[19]).

Nearly half of the calculated H_2 generation from the rods (~54 g for RUB-LEE), that means from still intact fuel rods and melt, is produced by the oxidation of intact fuel rod simulators (28 g for RUB-LEE) and the other half (26 g for RUB-LEE) is generated by melt oxidation.

The calculated mass of 54 g H_2 due to the oxidation of the fuel rod simulators represents about 73 % of the measured hydrogen from the rods (74 g; see [11]). The oxidation of the heat conducting (HECU) structures (Shroud and Grids for RUB-LEE) is clearly under-predicted due to the fact that the failure of these structures cannot be simulated using ATHLET-CD. The calculated mass of hydrogen of about 7 g from Shroud and Grids represents only 16 % of the measured 45 g of H_2 in the experiment. If only the hydrogen production from the oxidation of the intact inner side of the shroud at the heated length is considered (~8 g in the experiment), because only the inner oxidation of still intact HECU structures is calculable using ATHLET-CD, the under-prediction of the H_2 release by the oxidation of the shroud (approx. 6 g in the RUB-LEE calculation, Figure 11.1) amounts to nearly 25 % only (see [11]). This fact also reduces the measured global hydrogen release of calculable oxidation processes to 87 g leading to an under-prediction of approx. 30 % in the RUB-LEE calculation (see Ref. [17],[18],[19]).

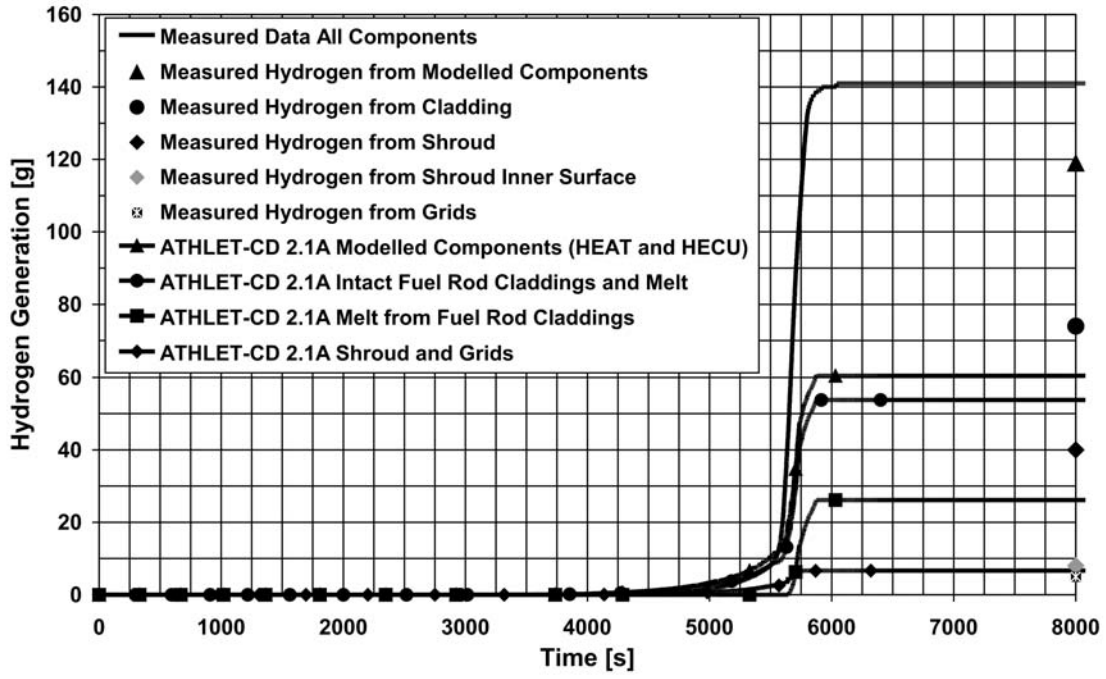

Figure 11.1: Measured and calculated hydrogen production (RUB-LEE results).

The kinetics of the oxidation reaction is simulated in good agreement with the measurements, even if the accumulated mass is under-estimated.

This under-estimation is mainly influenced by the oxidation of reactor untypical structures, i.e. shroud, because in using ATHLET-CD it is not possible to calculate the oxidation of the outer surface of the still intact shroud on the one hand. On the other hand melt oxidation of these HECU structures is not calculable, too (see Ref. [17],[18],[19]).

6.) These results as well as a comparison with other experiments and with other severe accident codes generally show a further demand for an improvement concerning oxidation of severe damaged structures during a reflood scenario (see Ref. [12], [17],[18],[19]).

10.2 Conclusions of the IBRAE Calculations / Results

The QUENCH-11 test represented an excellent challenge to investigate rod bundle behavior under boil-off and subsequent flooding conditions. It is the first test in QUENCH tests series with an initial water inventory and, therefore, it simulates the physical-chemical and mechanical phenomena in the real nuclear reactor core during a postulated severe accident with core uncovery and emergency water reflooding. It means that the QUENCH-11 experiment is a very valuable source of data for the verification of thermal hydraulic and SFD codes concerning the measures to control severe accidents at a nuclear power plant (NPP) with a pressurized water reactor (PWR).

For the IBRAE analysis of QUENCH-11 the Russian best-estimate thermal-hydraulics and SFD code RATEG/SVECHA was used. This code was developed for VVER severe accident analyses. Now, RATEG/SVECHA is a part of the integrated code system SOCRAT, which allows to perform a comprehensive calculation of a severe accident at a NPP of VVER design (including the aerosol behavior, phenomena in the containment, functioning of safety systems *etc*.) from the very beginning to the end of an accident (end-to-end modeling).

Modeling of the QUENCH-11 test by RATEG/SVECHA showed that the thermal-hydraulic behavior was reproduced pretty well by the code, taking into account a half-blind character of modeling. The calculated cladding temperature at 950 mm was approximately 100 K larger for the time interval 0-4800 s whereas the calculated shroud temperature at the same level and for the same interval was very close to the experimental values.

However, at times of 4800-5400 s, the calculation reveals obviously an overestimation of the cladding temperature of a maximum of 400 K. For the shroud temperature at the same times, the overestimation of the calculated results is considerably less (about 200 K). It is interesting, that on approaching the time of reflood initiation (5500 s) this discrepancy diminishes. This tendency is well reflected for the time of 5000 s and 5500 s, respectively. One can also see that many codes including RATEG/SVECVHA overestimated the temperature for the time of 5000 s for the level 550 mm to result in a deviation of more than 1000 K! The figures representing the axial temperature profile of rods and shroud at the time of 5490 s, confirm this statement.

For the IBRAE modeling, such a discrepancy is connected, at least partly, with the underestimation of water level in the bundle. This calculated underestimation began

approximately at a time of 1000 s and continued up to about 5000 s. Concerning the heat loss in the lower plenum we know that the value of heat loss in LP is a very sensitive parameter influencing directly the water level behavior by changing the water evaporation rate and indirectly the bundle temperature response. During the term of this benchmark exercise (summer and autumn of 2006) we did not take into account these heat losses adequately, so we overestimated the water evaporation rate and, hence, underestimated the water level in the bundle. Correspondingly, a premature temperature heat-up is observed in RATEG/SVECHA calculations, even at lower levels like 550 mm. Also, this resulted in a "flat-like" oxide layer thickness profile enveloping even the lower levels which is represented in our calculations (see Ref. [10]) in comparison to the experimental "classic" profile with a maximum at 950 mm.

Due to an overestimation of the calculated temperature before reflood, the hydrogen production before reflood (5500 s) is also overestimated in our calculations: 33.7 g in the calculations versus 8.1 g in the experiment.

We also have to mention the other reasons for temperature overestimation during the boil-off phase in RATEG/SVECHA calculations: too enlarged hydraulic diameter in the bundle channel (put into RATEG/SVECHA input file) and neglect of the radiative heat flux absorption in a steam medium in the bundle section. Both circumstances resulted in lowering of the heat transfer from the rods to the steam and consequently in additional heat-up of the bundle.

Considering the hydrogen generation during the reflood phase (5500÷6020 s), it is necessary to note that RATEG/SVECHA dramatically underestimated the hydrogen release at this phase (41 g in the calculations versus 133 g in the experiment) despite the fact that the maximum calculated temperatures are very close to the measured ones. Of course, such a behavior can partly be attributed to the following aspects:

- oxidation of non-prototypical materials was not modeled;
- spacer grids were not modeled;
- external oxidation of the shroud was not taken into account.

But, to be honest, the main reason for an underestimation of the hydrogen production is a RATEG/SVECHA intrinsic inability to estimate correctly the hydrogen release enhancement due to cracks formed in zirconia, and especially due to melt and debris oxidation under reflood conditions. We expect to improve the quality of modeling these phenomena will considerably improve the predictive ability of the code. The similar situation is typical for other codes, too, as one can see from the results of other participants on hydrogen production.

In conclusion, we can state, that, in our opinion, an adequate modeling of the heat loss from the lower plenum during the entire test and of oxidation of structures in a damaged geometry during the reflood are most important to get good results for QUENCH-11. Obviously, these two phenomena (heat loss from LP takes place even in "dry" QUENCH tests) are at least important for modeling of other QUENCH tests both performed and planned in future. The work to improve RATEG/SVECHA with respect to hydrogen generation during quench is currently underway.

10.3 Conclusions of the NRI Calculations

The application of the MELCOR 1.8.6 code to the QUENCH-11 experiment was, together with a tuning run of the QUENCH-01 test, the first application of this newly released version (in fall 2005). The development of an own input file for the QUENCH-11 test requested an application of new approaches, i.e. the bundle is practically full of water at the beginning of test with subsequent boil-off phase and the definition of an auxiliary heater in the bundle foot space.

The thermo-hydraulic phase was calculated by the MELCOR code sufficiently well and the collapsed water level evolution is in very good agreement with experiment values.

For the cladding failure temperature criterion the value of 2800.0 K was used. The value of 2500 K (default in MELCOR 1.8.6) corresponds to cladding failure as indicated in Phebus FPT-1 where the cladding-fuel pellet interaction resulted in an earlier failure than originally assumed (default in MELCOR 1.8.5 and earlier was 2800 K). So, the original value of this criterion, which was close to the ZrO_2 melting point, was reduced to the new value and is fitted to the FPT-1 results. And because the QUENCH facility does not use UO_2 fuel pellets, but ZrO_2 simulators, the user returned to this original value of 2800 K.

The input model for MELCOR 1.8.6 includes an application of a new code internal component “Shroud”, which was modeled in the previous version of the MELCOR code using a special trick to enable its oxidation. This new version enables to prepare the input model more easily without any special tricks. However, some trouble with the application of this new shroud component was identified and then reported to the developers to be finally solved in the version, which should be released at the end of 2007. The identified faults of the shroud model in the MELCOR 1.8.6 (releases YP and before) are following:

- There are no output variables related to the mass or thickness of oxide layer, independently for inner and outer surfaces. The output included two values of oxide masses, but there was an error in the written statement, which contains twice which in the beginning was understood by the user as unrealistic results on oxidation of inner and outer surfaces. Finally, it is possible to conclude that the shroud oxidation in the MELCOR 1.8.6 version is correctly calculated, independently for inner and outer surfaces, and it will be possible to check those results in the newly released version. The latest release (YR version) has a printed output correction with a sum of masses on inner and outer surfaces as a first step of bug fixing.

- The second trouble with new Shroud component was related to the degradation criteria assumed. The general coding of the MELCOR 1.8.6 in relation to the shroud component assumed that this component is supported by the former component structure. This former component is not generally requested to be included in the input, and such component is also not presented in the QUENCH facility. So, the correctly predicted melt-through of shroud at the elevation of 850 mm resulted in the collapse of all nodes of the shroud above the failure elevation due to an absence of a former support. This logical gap in the shroud model assumptions could be problematic also for some reactor applications, at least for the VVER-1000 core periphery modeling. This observation from the QUENCH-11 analysis was also reported to the developers, and the next release will

include a new specific input parameter, which will distinguish cases with the shroud supported by a former structure or it will enable to define a feature of a self-supporting shroud in each of its axial levels.

The most evident imperfection of the results predicted in the NRI calculation with the MELCOR 1.8.6 (YK version) code was a significant under-prediction of hydrogen generation – only about 33 g. The amount itself could not necessarily indicate a fault in the oxidation implementation in the code if it was possible to find reasons. A detailed analysis of the results was carried out and it showed the following important conclusions.

- The experiment results indicated full oxidation of cladding in the axial levels from 900 to 1300 mm. The NRI MELCOR check of the results was based on the mass balance approach for both Zr and ZrO_2. In the MELCOR calculations oxidation of the cladding contributed with 30.2 g, but the experiment results showed a value of 74 g. Calculation results showed that at the end of a computer run the only ZrO_2 that is presented lies in axial levels above 900 mm and it corresponds with the experiment. But the total amount of ZrO_2 in the levels above 900 mm corresponds to the oxidation of only 0.48 kg of Zr whereas the initial mass of Zr in those levels was 1.668 kg. More than 1 kg of Zr of the cladding candled relocating to levels below 900 mm; and only 1.65 % of this molten and candled Zr was oxidized. This is one of the most important reasons for the underestimation of hydrogen generation. Three main causes of this situation exist: (a) a low holdup of melt by the ZrO_2 shell, (b) too intensive downward progression of candling material, and (c) absence of melt oxidation. Concerning the first two causes, they could be eliminated by more accurate definition of appropriate input parameters and they are representative for a typical user effect. The third cause reflects the present lack of knowledge on melt oxidation kinetics to be implemented in such kind of a code.

- Only 1.5 g of hydrogen resulting from shroud oxidation was predicted, but the posttest examination showed about 40 g. The main reason for this underestimation is due to the collapse of the shroud component above the failure location at the time of 5512 s. The relocated material fell into the bypass region of the outer ring, which represents the annulus between shroud and isolation, and this space has pure argon atmosphere in the MELCOR analysis, so that the further oxidation of debris was terminated by the absence of steam. The code improvement in the shroud relocation logics would result in a better agreement with the experiment and also in continuing oxidation of the upper part of the shroud.

The MELCOR calculation over-predicted the downward propagation of melt or debris. This could be improved by tuning of the input parameters and this would be useful also for plant application, because the input parameters for candling and vertical relocation velocity of debris are input parameters with default values like for example a heat transfer coefficient for Zr upon solidification of 1000 W/m^2-K.

One can conclude from the MELCOR 1.8.6 application to this QUENCH-11 benchmark. The analysis showed a good capability to predict thermo-hydraulic behavior of bundle, to predict well enough the temperature evolution, but some imperfections in shroud modeling and unrealistic default values resulted in significant underestimation of the hydrogen generation. Observations about the code imperfections were reported to the developer team of the

MELCOR code. Recently, they were partly solved, and the remaining topics will be solved within the next version to be released at the end of 2007. This version will be applied to a recalculation of the QUENCH-11 test and then be approved for a plant analysis.

11 General Conclusions

The central part of the QUENCH program at Forschungszentrum Karlsruhe concerns integral tests about quenching or cooling an overheated reactor bundle by steam. QUENCH-11 was the first test to investigate the whole sequence of an anticipated reactor accident from the boil-off phase to delayed reflood with a low water injection rate. This ambitious experiment has been used as a basis for a SARNET benchmark for severe accident codes.

One of its dominant features is the well-known sensitivity of a two-phase flow system at low evaporation rate. One of the main tasks for the participants was therefore to correctly simulate the boil-off phase and in particular the heat losses to the environment (and later the quench phase which was the main aspect of previous QUENCH experiments). The development of the water level and the axial temperature and oxide profiles should therefore give an important insight of the performance of the calculation. The increased importance of thermal-hydraulic aspects with respect to other QUENCH tests also implied larger efforts than for previous tests even for those participants who are acquainted with this experimental program.

Results were delivered by ten participants of seven European countries and obtained with various worldwide-accepted detailed and integral severe accident codes. Evaluation of the results shows that for most variables a mainstream of results can be defined. Larger discrepancies are seen in the hydrogen production and the related oxide scale thickness. They can partly be attributed to less experienced users as it is well-known from other benchmarks that the skill of the code user to model a test and his understanding of the code plays an important role for the quality of the results. Experimental uncertainties and inherent limitations of the codes add to the differences in the results.

Since non-prototypical materials as electrodes are oxidized in the test, calculated hydrogen production cannot be compared directly to the measured value of 141 g, but should be compared to the value of 92 g that only includes contributions of reactor-prototypical components. Most calculated results are within a bandwidth of about 35 % of this value and hence not far from experimental error. For results that are higher than measurement, more oxidation is calculated before the quench phase. The impact of this error on results for the quench phase, however, cannot be assessed. One possible reason for underestimation might be the failure of the shroud during the quench phase which contributed to an enhanced oxidation in upper part of the bundle.

In the calculations with the different codes, the most sensitive input parameters were those concerning the auxiliary system - heater and water supply - and the electrical power release of the fuel rod simulators. The heat losses in the lower plenum and those through the shroud, especially above the heated region, have to be carefully simulated.

To assess which agreement with experimental data might be obtained at best in the calculations and experimental data, it is necessary to be aware of the purpose as well as of

the limitations of severe accident codes. They are intended and developed to analyze typical situations in reactors. To validate them, experiments are needed, but in integral tests like QUENCH-11, special features that are irrelevant for reactors cannot be simulated in the desirable detail. E.g., severe accident codes cannot simulate shroud failure with all its implications, and after such an event calculated results deviate more and more from measurements. At the best, a computer simulation is therefore only comparable with the experimental results up to shroud failure which occurred during the final part of the test.

An analysis of the experiment about its difficulties and limitations is equally important for this assessment. A number of weaknesses that inhibit better code evaluations are pointed out. They do not only concern inherent problems of this test but also uncertainties of experimental data. One of these uncertainties is also relevant in other QUENCH tests: temperature refers to electrical power release in the bundle. Presently, voltage measurement includes non-negligible parts of the circuit outside the bundle. In the participants' view and based on their experience with QUENCH tests in general, the situation can only be improved by appropriate experimental changes. For a better understanding of the test and perhaps for a better agreement with experimental data, further investigations of some uncertainties as heat losses, especially in the bottom part of facility, the external resistance of the heated rods and the axial power distribution at high temperature are necessary.

A comparison with other experiments not outlined in this report generally shows a further demand for an improvement concerning oxidation of severe damaged structures during a reflood scenario. Some limited code improvements and error corrections could be performed. In addition, the benchmark proved to be valuable for a number of participants to become acquainted with the physical problems and with the application of large severe accident codes. For the transfer of knowledge and experience to younger scientists and engineers, this is an important issue to maintain the standard of nuclear safety.

Having in mind the inherent limitations of severe accident codes to simulate complex tests like QUENCH-11, as well as the experimental uncertainties, the limited bandwidth of calculated mainstream results, including hydrogen is a good outcome of the code benchmark.

Acknowledgments

Using the Comparative Report on the OECD International Standard Problem ISP-45 (referred to the QUENCH-06 experiment [10]) as a guideline for this benchmark exercise proved to be very helpful.

Regarding ATHLET-CD analyses performed by RUB, the authors give specific acknowledgement to the German Federal Ministry of Economics and Technology (BMWi 150 1305) for their sponsoring.

The support of the IRSN ICARE/CATHARE calculations by Mr. G. Bandini, ENEA, Italy, is greatly appreciated as is the effort by Mrs. U. Stegmaier, FZK, to establish an experimental data base for the axial profiles of material distribution and fluid area.

References

[1] A. Miassoedov et al., “Large Scale Experiments on Core Degradation, Melt Retention and Coolability (LACOMERA),” FISA-2003: EU Research in Reactor Safety, Luxembourg, Nov. 10-13, 2003, Preproc., p. 239-244.

[2] ZIRCONIA Insulation Boards and Discs Types ZYFB-6 and ZYFB-3, Manufacturer’s data.

[3] J. Birchley, T. Haste and B. Jaeckel, “Calculational Support for the QUENCH-10 and QUENCH-11 Experiments,” Proceedings of the 11th International QUENCH Workshop, Karlsruhe, October 25-27, 2005 (CD-ROM).

[4] A. Stefanova et al., Internal report, 2006.

[5] www.fzk.de/quench/reports

[6] J. Stuckert et al.,“First results of the QUENCH-11 experiment,” SARNET 2nd Annual Review Meeting, PSI Villigen, January 30-31, 2006 (http://sarnet.grs.de/sites/WP9).

[7] W. Hering et al.,“Conduct and First Results of the QUENCH-11 Experiment,” Short note distributed per e-mail after the test, December 2005.

[8] W. Hering et al., ”Comparison and Interpretation Report of OECD International Standard Problem No. 45 Exercise (QUENCH-06)” FZKA 6722, Forschungszentrum Karlsruhe, 2002.

[9] W. Hering et al., ”Results of Boil-off Experiment QUENCH-11”, FZKA 7247, SAM-LACOMERA-D-18, Forschungszentrum Karlsruhe, Juni 2007.

[10] A. Stefanova et al., “Benchmark exercise on QUENCH-11 experiment”, European Review Meeting on Severe Accident Research, Karlsruhe, June 12-14, 2007.

[11] M. Steinbrück, “Analysis of Hydrogen Production in QUENCH Bundle Tests,” FZKA 6968, Forschungszentrum Karlsruhe, 2004.

[12] M. Steinbrück, W. Hering, J. Stuckert, J. Birchley, E. Brunet-Thibault, T. Drath, N. Seiler, K. Trambauer, M.S. Veshchunov, “Synthesis of the QUENCH program and its impact on code modeling,” 1st European Review Meeting on Severe Accident Research (ERMSAR-2005), Aix-en-Provence, France, 14-16 November 2005.

[13] Ch. Homann, W. Hering, “Analytical support for QUENCH-11,” M. Steinbrück, (editor), Proc. of the 12th International Workshop, Karlsruhe, CD-ROM, Karlsruhe, ISBN 978-3-923704-57-6, Forschungszentrum Karlsruhe GmbH, October 24-25, 2006.

[14] W. Hering, Ch. Homann, J. Birchley, B. Jaeckel, P. Groudev, A. Stefanova, “Preparation of QUENCH-11 with SCDAP/RELAP5, SCDAPSIM, MELCOR, and ASTEC,” FZKA 7305, Forschungszentrum Karlsruhe, in preparation.

[15] S.S. Kutateladze, V.M. Borishanskii, “Reference Book on Heat Transfer,” Moscow: Gosenergoizdat, 1969.

[16] T. Hollands, T. Drath, M. K. Koch, “First Results of the QUENCH-11 Benchmark Using ATHLET-CD,” Proceedings of the 12th International QUENCH Workshop 2006, Forschungszentrum Karlsruhe, October 2006, ISBN 987-3-923704-57-6.

[17] T. Hollands, T. Drath, H.-J. Wagner, M. K. Koch, “Results of the QUENCH-11 SARNET Benchmark Using ATHLET-CD,” Proceedings of the Annual Meeting on Nuclear Technology 2007, 1st Edition, CD Version, pp. 266-269, INFORUM Verlags- und Verwaltungsgesellschaft mbH Berlin, May 2007.

[18] T. Hollands, T. Drath, H.-J. Wagner, M. K. Koch, “Analysis of QUENCH-11 Experiment-Benchmark in the Framework of the EC-NoE SARNET Using ATHLET-CD,” 12th International Topical Meeting on Nuclear Reactor Thermal Hydraulics (NURETH-12), Proceedings, Paper P12, 30 Sep.-4 October 2007, Pittsburgh, PA, USA, ISBN 0-89448-058-8.

[19] T. Hollands, T. Drath, H.-J. Wagner, M. K. Koch, “Results of the QUENCH-11 SARNET Code Benchmark Using ATHLET-CD,” International Journal for Nuclear Power, atw 52 (2007), Vol. 12, pp. 791–798, INFORUM Verlags- und Verwaltungsgesellschaft Berlin, ISSN 1431-5254.